INTERNAL REPORT

HIP – 2003 – 2

Development of Radiation Hard Radiation Detectors – Differences between Czochralski Silicon and Float Zone Silicon

Eija Tuominen

Helsinki Institute of Physics, Helsinki, Finland

Dissertation for the degree of Doctor of Science in Technology to be presented with due permission of the Department of Electrical and Communications Engineering for public examination and debate in Auditorium S4 at Helsinki University of Technology (Espoo, Finland) on the 10th of October, 2003, at 12 o'clock noon.

ISSN 1455-0563
ISBN 952-10-1264-1

Acknowledgements

The research for this doctoral thesis was done between spring 2001 and spring 2003 while I worked as a Project Leader for Helsinki Institute of Physics (HIP) CMS Tracker Project at CERN, European Organization for Nuclear Research, in Geneva, Switzerland. My research work was partially funded by Magnus Ehrnrooth Foundation. Significant amount of the tasks were performed in collaboration with the Microelectronics Centre of Helsinki University of Technology and with the Department of Physics of University of Jyväskylä. I am most thankful to all these institutions.

This doctoral thesis materialized thanks to several colleagues from different institutes. I am most grateful to all the people who so devotedly participated in this research!

I would like to thank Professor Pekka Kuivalainen for his kind and supportive supervision of my post-graduate studies. I am grateful to Doctor Roland Horisberger and Doctor Simo Eränen for the thorough pre-examination of the manuscript of my thesis. I am indebted to my boss Professor Jorma Tuominiemi for his continuous confidence in my work and for his important encouragement, especially during the difficult moments.

My colleagues from HIP CMS Tracker Project form a magnificent detector research team. I am pleased to acknowledge my Instructor Jaakko Härkönen for so enthusiastically and professionally working with me with this thesis - and for being such a dear friend during the past years. I am thankful to Panja Luukka for volunteering whenever there is work to be done and so responsibly doing it; Donatella Ungaro for sharing the determination for completing a doctoral thesis; Sandor Czellar for providing experience in electronics; Esa Tuovinen for being responsible of the detector processing; Lauri Wendland for taking care of the beam tests; and Kati Lassila-Perini for visiting from the neighbouring project whenever help is needed.

Finally, I thank my parents, Eila and Pekka Tuominen, and my brother Jaska Tuominen, for their support and love.

Geneva, September 1st, 2003

Eija Tuominen

Abstract

The purpose of this work was to develop radiation hard silicon detectors. Radiation detectors made of silicon are cost effective and have excellent position resolution. Therefore, they are widely used for track finding and particle analysis in large high-energy physics experiments. Silicon detectors will also be used in the CMS (Compact Muon Solenoid) experiment that is being built at the LHC (Large Hadron Collider) accelerator at CERN (European Organisation for Nuclear Research). This work was done in the CMS programme of Helsinki Institute of Physics (HIP).

Exposure of the silicon material to particle radiation causes irreversible defects that deteriorate the performance of the silicon detectors. In HIP CMS Programme, our approach was to improve the radiation hardness of the silicon material with increased oxygen concentration in silicon material. We studied two different methods: diffusion oxygenation of Float Zone silicon and use of high resistivity Czochralski silicon.

We processed, characterised, tested in a particle beam, and irradiated silicon detectors and test structures. Samples were processed at the clean room facilities of Helsinki University of Technology Microelectronics Centre (MEC) where our group has the status of a member laboratory. Electrical characterisations were done mainly at CERN at the premises of our collaborators from CERN RD39 and RD50 research and development programmes, where our group is participating as a member institute. Defect characterisations were carried out using PCD (Photoconductivity Decay) and SPV (Surface Photovoltage) methods at Helsinki University of Technology Electron Physics Laboratory. Detection performance was measured with a Helsinki Silicon Beam telescope at CERN using muon beam. Radiation hardness was studied in irradiation tests at Jyväskylä University Accelerator Laboratory.

Our research on the radiation hardness of diffusion oxygenated Float Zone silicon resulted in several previously unreported findings. We found an evident correlation between silicon oxygenation and detector leakage current after irradiations. Additionally, we found that the oxygenation has a positive effect on the long-term stability of irradiated silicon. Furthermore, we successfully applied alternative methods for the characterisation of silicon detectors, i.e. PCD (Photoconductivity Decay) and SPV (Surface Photovoltage).

The most important results of our research were obtained in our work on high resistivity Czochralski silicon. Although the advantages of Czochralski silicon had been known for some time, we were the first group to process, characterise, test in a particle beam, and irradiate full-size Czochralski silicon detectors. In proton irradiations, Czochralski silicon was found to be more radiation hard than any other silicon material.

List of Publications

I J. Härkönen, E. Tuominen, K. Lassila-Perini, M. Palokangas, M. Yli-Koski, P. Heikkilä, V. Ovchinnikov, L. Palmu, and S. Kallijärvi, *Processing and recombination lifetime characterisation of silicon microstrip detectors*, Nuclear Instruments and Methods in Physics Research **A485** (2002) 159-165.

II J. Härkönen, E. Tuominen, E. Tuovinen, K. Lassila-Perini, S. Nummela, J. Nysten, P. Heikkilä, V. Ovchinnikov, M. Palokangas, M. Yli-Koski, L. Palmu, S. Kallijärvi, T. Alanko, P. Laitinen, A. Pirojenko, I. Riihimäki, G. Tiourine, and A. Virtanen, A., *The effect of oxygenation on the radiation hardness of silicon studied by surface photovoltage method*, IEEE Transactions in Nuclear Science **49** (6) (2002) 2910-2913.

III J. Härkönen, E. Tuominen, E. Tuovinen, K. Lassila-Perini, S. Nummela, J. Nysten, P. Heikkilä, V. Ovchinnikov, M. Palokangas, M. Yli-Koski, L. Palmu, S. Kallijärvi, T. Alanko, P. Laitinen, A. Pirojenko, I. Riihimäki, G. Tiourine, and A. Virtanen, *Annealing study of oxygenated and non-oxygenated Float Zone silicon irradiated with 15 MeV protons*, Nuclear Instruments and Methods in Physics Research A (in press).

IV J. Härkönen, E. Tuominen, E. Tuovinen, P. Heikkilä, V. Ovchinnikov, M. Yli-Koski, L. Palmu, S. Kallijärvi, H. Nikkilä, O. Anttila, *Processing microstrip detectors on Czochralski grown high resistivity silicon*, Nuclear Instruments and Methods in Physics Research A (in press).

V E. Tuominen, K. Banzuzi, S. Czellar, A. Heikkinen, J. Härkönen, P. Johansson, V. Karimäki, P. Luukka, P. Mehtälä, J. Niku, S. Nummela, J. Nysten, J. Simpura, E. Tuovinen, J. Tuominiemi, D. Ungaro, T. Vaarala, L. Wendland, M. Voutilainen, A. Zibellini, *Test beam results of a large area strip detector made on high resistivity Czochralski Silicon,* Nuclear Physics B (Proceedings Supplements) 125 C (2003) 175-178.

VI E. Tuominen, J. Härkönen, E. Tuovinen, K. Lassila-Perini, P. Luukka, P. Mehtälä, S. Nummela, J. Nysten, A. Zibellini, Z. Li, P. Heikkilä, V. Ovchinnikov, M. Yli-Koski, P. Laitinen, I. Riihimäki, and A. Virtanen, *Radiation Hardness of Czochralski Silicon Studied by 10 MeV and 20 MeV Protons*, Submitted for publication: IEEE Transactions in Nuclear Science. Currently available: Helsinki Institute of Physics HIP-2003-17/EXP (2003) 4 pp.

VII K. Banzuzi, S. Czellar, A. Heikkinen, J. Härkönen, V. Karimäki, M. Leppänen, P. Luukka, S. Nummela, E. Pietarinen, E. Tuominen, J. Tuominiemi, and L. Wendland, *Test beam results with upgraded Helsinki Silicon Beam telescope*, Helsinki Institute of Physics HIP-2001-08 (2001) 27 pp.

Brief description of the contents of the publications

Publication I describes our process in the manufacture of silicon strip detectors. Additionally, Publication I demonstrates the suitability of the microwave Photoconductive Decay (μPCD) method for the characterisation of silicon devices.

Publication II demonstrates that diffusion oxygenation improves the radiation hardness of Float Zone silicon, seen in both minority carrier diffusion length and diode reverse current measurements. The irradiations were made with 15 MeV protons.

Publication III describes an annealing study demonstrating that diffusion oxygenation reduces the long-term instability of irradiated silicon. Additionally, Publication III demonstrates the suitability of the Surface Photovoltage Method for the characterisation of irradiated silicon devices.

Publication IV introduces the first large area strip detectors ever processed on high-resistivity Czochralski Silicon. Publication IV describes the processing method and presents the results of lifetime characterisation using the PCD method, defect characterisation using the DLTS method, and electrical characterisation using current-voltage and capacitance-voltage measurements.

Publication V demonstrates that our Czochralski detectors act as particle sensors with appropriate resolution, efficiency, and signal-to-noise ratio. This study was carried out with an HIP Silicon Beam Telescope (SiBT).

Publication VI demonstrates the outstanding radiation hardness of high-resistivity Czochralski silicon, studied with 10 and 20 MeV protons.

Publication VII explains the principle of the HIP Silicon Beam Telescope (SiBT) at the CERN H2 test beam. The updates carried out for the summer 2001 beam tests are described.

Author's contribution

My specific responsibility in this investigation on radiation hard silicon detectors has been the general coordination of our research activities. I have participated personally in most of the different activities of this study, i.e. research planning, electrical characterisation, irradiations, beam tests, data analysis, reporting, fund raising and, to a minor extent, device processing. I wrote Publications II, III, IV, V and VI with Jaakko Härkönen and I participated in the writing of Publications I and VII.

Table of Contents:

Acknowledgements iii

Abstract vi

List of Publications v

Table of Contents vii

1 Introduction 1

1.1 Motive 1

1.2 Approach 2

1.3 Methods 3

2 Research methods 5

2.1 Device processing 5

2.2 Electrical characterisation 7

2.3 Lifetime using the Photoconductivity Decay(PCD)method 7

2.4 Diffusion length using the Surface Photovoltage (SPV) method 11

2.5 Detection properties using a Silicon Beam Telescope 13

2.6 Irradiations 16

3 Effect of oxygenation on the radiation hardness of Float Zone silicon 17

3.1 Sample processing and irradiations 17

3.2 Effect of oxygenation on the diffusion length of silicon 18

3.3 Effect of oxygenation on the leakage current of silicon 19

3.4 Suitability of SPV for characterising irradiated silicon 20

3.5 Effect of oxygenation on the long term stability of irradiated silicon 20

4 Czochralski silicon as material for radiation hard particle detectors 24

4.1 Why high resistivity Czochralski silicon? 24

4.2 Crystal growth of Czochralski silicon 25

4.3 Processing Czochralski silicon detectors 25

4.4 Lifetime of minority charge carriers 26

4.5 Defect characterisation 27

4.6 Detector characterisation 29

4.7 Performance of Czochralski silicon in particle detection 31

4.8 Irradiations 32

5 Conclusions 34

References 35

1 Introduction

1.1 Motive

The main objective of this work was to improve the radiation hardness of high resistivity silicon. Radiation detectors made of high resistivity silicon are cost effective and have excellent spatial resolution, Fig. 1.1. Therefore, they are widely used for track finding and particle analysis in particle physics experiments. Silicon detectors will also be used in the CMS (Compact Muon Solenoid) experiment that is being built at the LHC (Large Hadron Collider) accelerator at CERN (European Organisation for Nuclear Research). Both CMS and LHC are scheduled for 2007. The CMS Tracker sub-detector will house 220 m^2 silicon detectors. Detectors and adjacent electronics will be mounted on lightweight support frames, or rods, and installed in a cylindrical support wheel, Fig. 1.2.

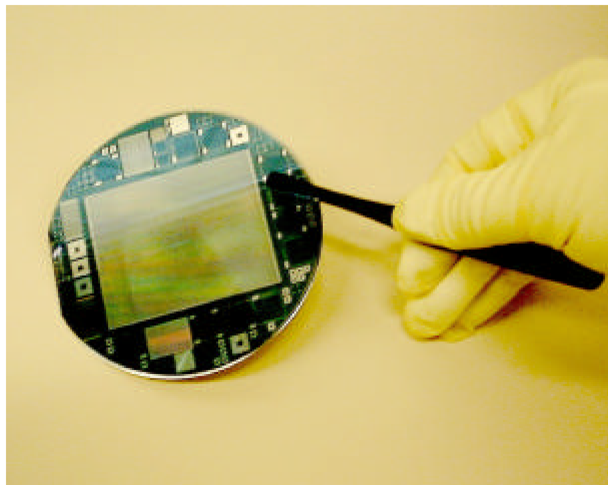

Figure 1.1. Radiation detector and test structures processed on a silicon wafer.

Exposure of the silicon material to particle radiation causes irreversible defects that diminish the performance of the silicon detectors. Thus, improving the radiation hardness of the detectors is a very important research subject in experimental particle physics [1]. For example, the irradiation dose in CMS Tracker will be significantly higher than in any previous high-energy physics experiment [2, p. 12].

Silicon detectors are pn-junction devices operating at full depletion. Radiation induced defects diminish the performance of the silicon devices in two principal ways. First, in the silicon material, the defects create generation-recombination centres that decrease the minority carrier diffusion length and increase the leakage current with relation to the irradiation dose [3]. Thus, the electrical signal created by the particle traversing the detector becomes difficult to distinguish from the background noise.

Figure 1.2. Tommi Vanhala inserting prototype support frames with silicon detectors in a prototype CMS Tracker Outer Barrel support wheel.

Second, lattice defects change the effective resistivity of the silicon. Consequently, the operating voltage needed for the full depletion of the detector changes and gradually may exceed the breakdown voltage of the device. Additionally, as the irradiation dose increases, the defects eventually change the type of conductivity of the silicon from n-type to p-type.

The deterioration of the silicon detectors in particle radiation is the most serious limitation of the long-term performance of large modern particle physics experiments. Thus, all the results obtained in the improvement of radiation hardness of silicon detectors are directly applicable to the international community of high-energy physics, including future CERN experiments. In addition, the results can be exploited in space research since similar detectors are used to measure high particle radiation fields in space.

1.2 Approach

A widely studied approach to improve the radiation hardness of silicon detectors is to introduce oxygen into the silicon material [4]. The oxygenation has been reported to slow changes in silicon resistivity, but no effects on the leakage current had been observed before our work [5].

Silicon strip detectors have traditionally been processed using so called Float Zone silicon (Fz-Si). Because of the high resistivity of the Fz-Si, full detector depletion can be achieved at reasonable operating voltages. However, the Fz-Si has a low oxygen concentration. Because of the silicon contamination risk present in high temperature processes, the diffusion oxygenation of the Fz-Si is very difficult to implement on a large scale.

Silicon wafers made using the so-called Czochralski (Cz) method intrinsically contain high concentrations of oxygen. On the other hand, the resistivity of the Cz-wafers is typically not high enough for detector applications. However, recent developments in the crystal growth technology of Czochralski silicon (Cz-Si) have enabled the production of Cz wafers with sufficient resistivity and with well-controlled, high concentration of oxygen. Before our work, there had been no scientific reports on silicon detectors that have been made essentially more radiation tolerant by adding impurities during crystal growth.

In this work, we have studied the radiation tolerance of particle detectors processed on diffusion oxygenated Float Zone silicon as well as detectors processed on Czochralski silicon. In addition, we have studied the suitability of PCD (Photoconductivity Decay) and SPV (Surface Photovoltage) methods for the characterisation of irradiated silicon detectors.

Our research was conducted in the framework of two large CERN R&D Programs. "Development of radiation Hard Semiconductor Devices for Very High Luminosity Colliders", or RD50, is a collaboration of some 50 institutes including HIP. The objective of the collaboration is to develop feasible detector solutions for future high-energy physics experiments where the irradiation field will be an order of magnitude higher compared to the actual experiments [6]. Our group at HIP is also participating in the collaboration "Detectors at the Cryogenic Temperatures", or RD39, which studies the possibility of extending the lifetime of detectors in a hostile radiation environment by cooling them to very low temperatures [7].

1.3 Methods

The detectors were processed at the clean room and fabrication facilities at the Microelectronics Centre (MEC) of Helsinki University of Technology (HUT), Fig. 1.3. In 2001, the Helsinki Institute of Physics (HIP) CMS Program became a member of MEC. The capability to produce silicon detectors and test structures is exceptional in the high-energy physics community.

Figure 1.3. Processing: Jaakko Härkönen loading silicon wafers into an oxidation furnace at the MEC clean room.

Some preliminary electrical characterisations, i.e. current-voltage measurements, were carried out at the Helsinki University Kumpula Campus where HIP has clean room facilities, Fig. 1.4. However, current-voltage characteristics were mainly measured at Oulu University Microelectronics Instrumentation Laboratory. The capacitance-voltage measurements to characterise the detector depletion voltage were performed at CERN at the premises of our collaborators from the RD39 and RD50 programmes. Additionally, after being able to start the C-V measurements, we also performed the I-V measurements at the laboratories of our CERN collaborators. Furthermore, we studied the minority carrier recombination lifetime using the PCD (Photoconductivity Decay) method, and the minority carrier diffusion length using the SPV (Surface Photovoltage) method. This equipment was kindly provided by Helsinki University of Technology Electron Physics Laboratory.

The detection performance was measured at the HIP Silicon Beam telescope at the CERN H2 beam station, Fig. 1.5. HIP SiBT is an outstanding tool for measuring detector efficiency and signal-to-noise ratio in real LHC-like conditions. HIP had two weeks of beam time during the summers of 2001 and 2002.

The radiation hardness properties of the detectors were studied in irradiation tests at Jyväskylä University Accelerator Laboratory in November 2001, October 2002 and December 2002, Fig. 1.6. The irradiations were performed in cooperation with Jyväskylä RADEF (RADiation Effects Facility) group.

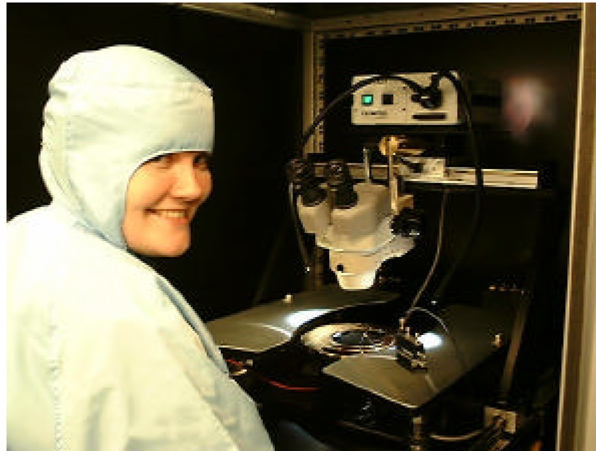

Figure 1.4. Characterisation: Panja Luukka measuring I-V characteristics of a silicon detector at HIP clean room.

Figure 1.5. Detection: Lauri Wendland programming SiBT Data Acquisition at the CERN H2 beam station.

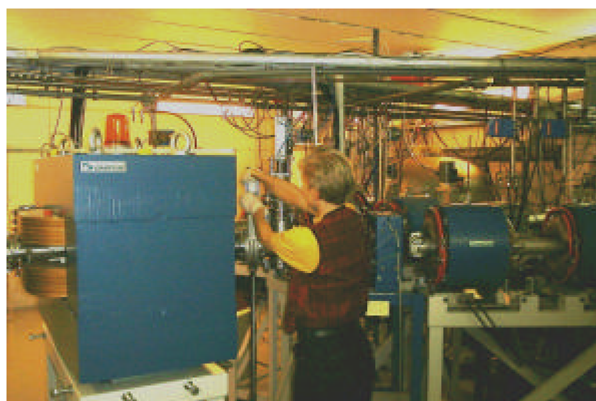

Figure 1.6 Irradiations: Eija Tuominen preparing the RADEF beam line for changing of sample at Jyväskylä University.

2 Research methods

2.1 Device processing

Silicon detectors are reverse biased pn-junction diodes working at full depletion. For position sensitivity, the p-side of the junction is divided into an array of one-dimensional strips or two-dimensional pixels. In silicon microstrip detectors, the width of one strip is typically around ten micrometers and the separation between the neighbouring strips some tens of micrometers, depending on the desired resolution. When a charged particle passes through the silicon detector, it generates electron-hole pairs. The holes drift in the electric field towards the negatively biased p-strips and are collected as a charge pulse to the readout electronics. Since the holes drift to the strip nearest to their point of generation, the position of the particle impact is obtained.

We made silicon strip detectors at the clean room facilities of Microelectronics Centre of Helsinki University of Technology. Our detector fabrication process contains four mask levels and consists of two thermal oxidations, two ion implantations, and three sputter depositions. The detector size at our most-used design was 32.5 cm^2. In addition, test structures were processed on the edges of the wafer. We processed AC-coupled p^+nn^+ devices on 4” phosphorous-doped n-type silicon wafers from different manufacturers.

Masking oxide (first oxidation)

Prior to any high-temperature processing, the silicon wafers were always cleaned using the RCA (Radio Corporation of America) method in order to remove organic and inorganic impurities from the surface [8]. The quality and purity of the high-temperature thermal oxidation is the most demanding aspect in the silicon processing. The metallic contamination present during the oxidation determines the leakage current of detectors. For example, the iron present in a one-euro-coin is able to contaminate the production of the entire world’s microelectronics industry for one year [9].

The first processing step was the growth of the silicon dioxide (SiO_2) layer. This field oxide layer would act as a mask for the ion implantation of the p-type strips. Additionally, the oxide protects the non-active area from contamination during processing. The oxidation was carried out in a horizontal quartz tube furnace in dry oxygen atmosphere at a temperature of 1050°C. The thickness of our most-used silicon dioxide layer was 250 nm, when the growth lasted for about eight hours. Relatively slow temperature ramp-up and cool-down rates were used in order to avoid the slip defect formation.

p^+ strips and n^+ backside (first photomask)

The openings for the front side p+ strips were patterned by photolithography using the first level photomask in a mask-aligner. The strips were opened to the silicon oxide by wet etching using Hydrogen Fluoride (HF) acid that removes the silicon oxide but does not essentially affect the silicon underneath. Since sharp edges may potentially cause high electric fields during the reverse bias operation of the detector, in our most-used design the ends of each strip were rounded as shown in Fig. 2.1.

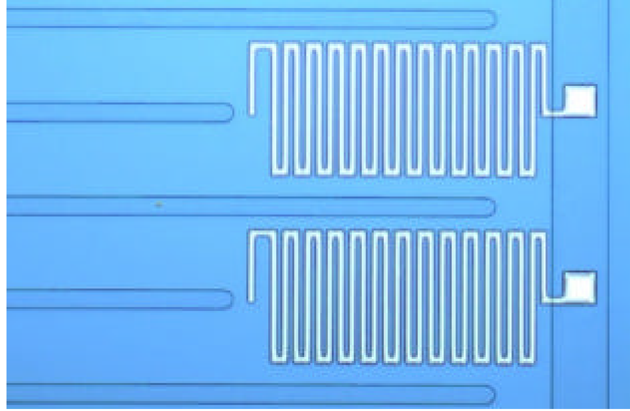

Figure 2.1. Partial microscopic picture of a strip detector after two lithography levels. The ends of each strip are rounded in order to avoid high electric fields during the detector operation. In addition, bias resistors are shown in the picture.

The strips were implanted with 30 keV boron ions. The width of the strip in our most-used design was 10 μm and the length 6.159 cm. The pitch width was 50 μm. Immediately after the strip implantation, the n^+ area at the detector back surface was implanted with 70 keV phosphorous ions. The implantation dose for both boron and phosphorous ions were 10^{15} cm^{-2}.

AC-coupling and bias resistors (second oxidation and second photomask)

Dielectric SiO_2 film for isolating the AC-coupled signal strips was grown using dry thermal oxidation at a temperature of 1050°C. At this temperature, it takes five hours to grow a 200 nm thick SiO_2 film.

Simultaneously, five hours of heat treatment, with additional thermal load from the temperature ramp-up and ramp-down, provides a drive-in diffusion for the front side boron and the rear side phosphorous implants. In our most used recipe, the temperature ramp-up velocity was 15°C per minute and the ramp-down velocity was 4°C per minute. The resulting depths of the p^+ and n^+ implants were around four micrometers, estimated using a one-dimensional process simulator [10].

The integrated bias resistors were patterned to the sputtered metal using the second mask level. The implanted p^+ strips are connected via resistors to the p^+ well region that will be biased with operating voltage during the detector operation. The unique feature of our detector process was the bias resistors made by reactive magnetron sputtering of tungsten nitride (WN_x).

Non–stoichiometric tungsten nitride, WN_x, has been extensively studied as a candidate for diffusion barrier material for very large-scale integrated circuit (VLSI) metallization applications. The main reason for choosing this material for the thin film resistors was to simplify the fabrication process. For instance, WN_x can be deposited at room temperature thus reducing the possibility of contamination or defect formation that may take place during high temperature processing. Additionally, WN_x can be selectively wet etched with hydrogen peroxide. The resulting clear-cut resistor structures can be seen in Fig. 2.1. The resistivity of the deposited film depends on the sputtering conditions and a value of 20 μΩcm has been reported within the nitrogen content $10\% < x < 45\%$ [11].

Metallic contacts (third and fourth photomask)

The third photo-mask level was used to provide an etching mask for opening contact holes for the p^+ strips through the SiO_2 layer. The contact holes are 5 μm * 5 μm rectangular squares adjacent to the bias resistors. The silicon dioxide was etched with HF solution.

The fourth photo-mask level was used for patterning the aluminium metallization. Aluminium is wet etched with a commercially available etching solution (Merck PS 70-10). A 2 μm overhang of the aluminium metallization was designed over the strip implant. The overhang influences the electric field near the strips, thus decreasing the possibility of break-through at higher bias voltages. This in turn results in higher breakdown voltages of the silicon detector [12].

After the patterning of the front side metallization, the aluminium was sputter deposited to the rear of the detector wafers. The final process step was the sintering of the aluminium contacts in a quartz tube furnace in N_2 atmosphere for 15 minutes, at a temperature of 450° C in the case of Float Zone silicon and at 350° C in the case of Czochralski silicon (because of its higher oxygen concentration).

2.2 Electrical characterisation

Current voltage (IV) and capacitance voltage (CV) measurements are important tools in the study of the effects of irradiation in silicon. Current voltage measurements were carried out in order to study the leakage currents of the detectors. Currents were typically measured up to high operating voltages, at least up to the detector depletion voltage, in order to verify the lack of detector breakdown. IV characteristics were measured both from test diodes and from full-size detectors.

Capacitance voltage measurements gave the value of the detector depletion voltage. CV characterization was done to test diodes processed simultaneously with full-size detectors. Capacitances were typically measured with the frequency of 10 kHz. Higher frequencies proved to unpractical, probably since the frequency of the emission from the charge carrier traps is relatively low and the capacitance should be measured only when the slow traps were emptied. On the other hand, lower measurement frequencies increase the 1/f noise.

We used a semi-automatic probe station with parameter analysator to measure the electrical properties of the silicon devices. The probe station is inside a black box blocking light from the sample to be measured. The measurement set-ups were relatively simple without thermal jig or dry nitrogen flux. The electrical characterisations were mainly done at the laboratories of our collaborators at CERN.

Since the beginning of our research, the current voltage measurements showed very promising results. The leakage currents of our detectors were at the same low level as requested from the leading European semiconductor manufacturers currently providing detectors for the CERN experiments. Later, i.e. after joining CERN RD39 and RD50 programmes, we obtained access to capacitance-voltage measurement unit.

2.3 Lifetime using the Photoconductivity Decay (PCD) method

Minority carrier lifetime is a key parameter in determining the quality of silicon processing. Despite the clean process conditions, there is always a possibility for metallic process-induced contamination, e.g. iron and copper, decreasing the lifetime and increasing the leakage current. The contamination control during the processing of large area devices is essential. In addition to metallic impurities, process induced defects may increase the device leakage current. Since a particle detector typically consumes at least 50 % of the surface of a silicon wafer, even a minor defect or a localised metallic contamination might lead to poor operational characteristic of the detector.

We monitored the minority carrier recombination lifetime using the PCD (Photoconductivity Decay) method, which is a practical method for device characterisation since it does not require electrical contacts. We studied the suitability of the PCD method for the characterisation of silicon detectors. In particular, we were interested in the correlation between the charge carrier lifetime and the detector leakage current.

Principle of the μPCD method

In this method, the silicon sample is illuminated with a short laser pulse. The wavelength of the monochromatic light is chosen so that the light is absorbed within the volume of the sample. The recombination of the excess electron-hole pairs, generated by the light, decreases the conductivity of the sample. The transient in the conductivity is measured using the reflectance of a microwave signal, proportional to the electrical conductivity of the material under investigation. The principle of the PCD measurement is described in detail in Ref. [13, pp. 429-437]. The PCD measurement returns a parameter known as effective lifetime, which is a complex combination of effects of recombination processes in both the sample surface and the bulk. However, the surface recombination must be effectively suppressed in order to measure accurately the bulk lifetime. Therefore, the minority carrier lifetimes are measured using wafers electrically passivated by thermally grown silicon oxide.

The concentration of excess carries generated by the laser pulse decays exponentially with the effective lifetime [13]:

$$\Delta n(t) = \Delta n(0) e^{-\frac{t}{\tau_{eff}}} , \tag{2.1}$$

where t is time and the effective lifetime τ_{eff} is given by:

$$\frac{1}{\tau_{eff}} = \frac{1}{\tau_B} + D\beta^2 , \tag{2.2}$$

where τ_B is bulk lifetime, D is diffusion coefficient and parameter β is defined as:

$$\beta \tan(\frac{\beta T}{2}) = \frac{s_r}{D} , \tag{2.3}$$

where T is the thickness of the sample, and s_r is surface recombination velocity.

As seen in Eqs. (2.2) and (2.3), the result of the PCD measurement, i.e. the effective lifetime, is a non-linear combination of recombination processes occurring both in the silicon bulk and at the wafer surfaces. Therefore, in the PCD measurement the surface recombination effect must be suppressed effectively. For example, high-temperature dry oxidation produces a SiO_2-Si interface with a very low electrical activity.

In this μPCD measurement unit, the minority carriers are excited by a 902 nm pulsed laser operating at cycles of 200 ns. During the measurements, the power of the laser was kept constant so that the laser injected approximately 10^{16} electron-hole pairs per cubic centimetre. The frequency of the microwave signal was between 10 and 11 GHz and was adjusted separately for each sample in order to achieve the highest possible reflected signal from decaying minority carriers.

The leakage current of the strip detector is a generation current caused by the generation-recombination (G-R) centres that are impurities or defects. Thus, the density of the leakage current can be expressed as:

$$J_{Gen} = \frac{q n_i W}{\tau_g} , \tag{2.4}$$

where q is elementary charge, n_i is intrinsic carrier concentration, and W is the width of the depletion region. At full depletion ($V = V_{fd}$), W is equal to the thickness of the silicon wafer. The parameter τ_g is generation lifetime given by [14, p.90]:

$$\tau_g = \frac{2\cosh\left(\frac{E_T - E_i}{kT}\right)}{\sigma_0 v_{th} N_T}, \tag{2.5}$$

where E_T is the energy level of the centre, E_i the intrinsic Fermi level, k is the Boltzmann constant, T temperature, σ_o the capture cross section of the trap, v_{th} thermal velocity and N_T is the concentration of traps. According to Ref. [15], the following relation exists between recombination and generation lifetimes:

$$\frac{\tau_g}{\tau_r} = 2\sqrt{\frac{c_p}{c_n}}\cosh\left(\left(\frac{E_T - E_i}{kT}\right) + 0{,}5\ln\left(\frac{c_n}{c_p}\right)\right), \tag{2.6}$$

where $c_{n,p}$ are capture rates for electrons and holes, respectively. In addition, τ_r is the recombination lifetime quoted in Eq. (2.2) as the bulk lifetime τ_B. Thus, Eq. (2.6) can be significantly simplified if a symmetric capture is assumed for electrons and holes:

$$\frac{\tau_g}{\tau_r} \approx e^{\left(\frac{E_T - E_i}{kT}\right)}. \tag{2.7}$$

According to Eqs. (2.4 - 2.7), there is a theoretical dependence between the detector's density of leakage current and the recombination lifetime, as illustrated in Fig. 2.2. This calculation is based on the ideal model, and thus the dependence shown in Fig. 2.2 should be considered as the minimum value for leakage current. Other mechanisms such as edge leakage currents or leakage current due to surface recombination are excluded.

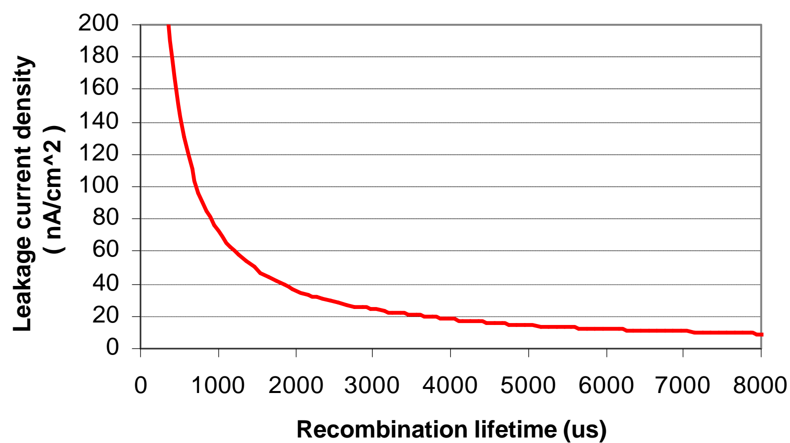

Figure 2.2. Dependence between leakage current density and recombination lifetime. The width of depletion region is assumed to be 300μm and E_T-E_i is -0,05 eV corresponding the deep level caused by iron [14].

The PCD method for characterisation of silicon detectors

In order to study the reliability of the theoretical predictions shown in Fig. 2.2, three sets of detectors were processed on 300 μm thick 4" wafers with a resistivity of 5000 Ωcm. Lifetime was measured from the monitor wafers of each set, after the first oxidation step. Values for the leakage current density were measured from the completed detectors. The results are shown in Table 2.1.

Table 2.1. The average lifetimes measured by PCD and the leakage current densities for the three processing batch. The batch size was five wafers for A and B and eight for C. Some wafers were lost because of breakage during the processing.

Processing batch	Average lifetime μs	Leakage current density @ 40V (several monitor wafers) nA/cm^2
A	300	52.9
		142
		125
		1010
		106
B	4300	10.3
		293
		13.9
C	6500	5.5
		5.9
		14.6
		9.0
		12.7
		5.7

We assume that the differences in the values of the leakage current inside one processing batch are due to process-induced defects such as surface scratches that could not be identified by optical inspection. For example, batch B contains only three finished detectors of which one is much worse than the other two. On the other hand, the differences between different batches are caused by different processing conditions, such as the purity of the deionised water used in the processing. For example, batch A detectors show higher leakage current as well as poorer lifetime values due to water contamination problem.

We assume that the differences in the values of the leakage current inside one processing batch are due to process-induced defects such as scratches. On the other hand, the differences between different batches are caused by different processing conditions, such as the purity of the deionised water used in the processing.

The recombination lifetime measured using the μPCD method is not the low-level injection minority carrier lifetime derived in the famous Schockley-Read-Hall (SRH) theory. The lifetime measured under high-level injection conditions ($\Delta p >> n_0$) seems, however, to correlate with the leakage current of detectors. According to the SRH-theory, the lifetime increases with the increasing injection level. This has been experimentally observed in many reports. In p-type silicon, this behaviour is strengthened by the presence of iron, the most common impurity in p-type samples. Iron exists in p-type silicon as an interstitial (Fe_i) or is paired with boron (Fe_B). High-level injection tends to break the iron-boron pairs to the Fe_i that in turn exhibits strong recombination activity dependence on the injection level [16]. The interpretation of the injection level dependence of the lifetime in n –type silicon is somewhat more difficult. For instance, in Ref. [17] experimental data show that the recombination lifetime remains practically unchanged over the three orders of magnitude of the injection level.

The high-level injection during the lifetime measurement also influences the effective surface recombination velocity. Since the measured recombination lifetime depends on the bulk and surface recombination, the interpretation of the results becomes more difficult [18].

Apparently, there is a good agreement between the measured leakage current values and the theoretical prediction presented in Fig. 2.2. Thus, in order to achieve leakage current values as low as 5 - 6 nA/cm^2, the minority carrier lifetime must be as high as 6000-8000 µs. On the other hand, a lifetime of 1000 µs or less in the completed device results in leakage current of 100 nA/cm^2 or more.

2.4 Diffusion length using the Surface Photovoltage (SPV) method

Surface Photovoltage (SPV) method was first reported in ref. [19]. Nowadays, SPV has been successfully implemented as a tool for process monitoring and contamination control in the microelectronics industry. In this method, a silicon sample, e.g. oxidized silicon wafer, is illuminated with monochromatic light with energy larger than that of the silicon band gap. The charge carriers generated by the light diffuse to the illuminated surface. The space charge electric field present near the silicon surfaces separates the positive and negative charge carriers. The separated charge carriers create a surface potential V_{SPV} that is, within certain limits, linearly proportional to the number of excess charge carriers generated by light at the edge of the space charge region. An expression for V_{SPV} can be derived from the semiconductor continuity equations and realistic boundary conditions [19]:

$$V_{SPV} = \frac{\left(\frac{kT}{q}\right)(1-R)\Phi L_n}{n_{p0}\left(s_1 + \frac{D_n}{L_n}\right)\left(L_n + \frac{1}{\boldsymbol{a}}\right)}, \tag{2.8}$$

where k is the Boltzmann's constant, T temperature, q the elementary charge, R the relative reflectance of the sample surface, $\boldsymbol{F}$ the photon flux, L_n the diffusion length of minority carriers, n_{p0} the concentration of minority charge carriers at the edge of the space charge region, s_1 is the recombination velocity at the edge of the space charge region near the front surface of the sample, D_n the diffusion constant of minority carriers, and α the absorption coefficient of the incident light. Eq. (2.8) is derived for p-type semiconductor where electrons are minority carriers. A similar equation applies for n-type semiconductors.

During the sample illumination, the surface potential V_{SPV} is kept constant. Thus, if the sample is illuminated by at least two light sources with different wavelengths, a different photon flux $\boldsymbol{F}$ is needed to create a constant surface potential. The diffusion length L_n can be extracted if the photon flux is plotted as a function of the penetration depth, i.e. the inverse of the absorption coefficient, of the illuminating light. For simplicity, the recombination velocity s_1, the reflectance of the sample surface R, the diffusion coefficient of minority carriers D_n, the constant surface potential V_{SPV}, and the temperature T in Eq. (2.8) can be presented by a constant C. Thus, a simplified expression for the Eq. (2.8) is [19]:

$$\Phi = C\left(L + \frac{1}{\boldsymbol{a}}\right), \tag{2.9}$$

where $\boldsymbol{F}$ is the photon flux, L the diffusion length of minority carriers, and $\boldsymbol{a}$ the absorption coefficient of the incident light. A comprehensive mathematical analysis of the SPV method can be found e.g. in Ref. [13, pp. 485-493]. The principle of this measurement technique is schematically illustrated in Fig. 2.3.

The SPV method is an effective method for characterisation of irradiated silicon samples. As can be seen in Eq. (2.9), the surface recombination related term s_1 is included in the constant C and does not need to be known. Since the particle radiation degrades both the surface and the bulk properties of silicon, the exclusion of surface effects is of vital importance for studying radiation damage in silicon [20], otherwise the measurement gives a value that is an undetermined combination of bulk lifetime and surface recombination.

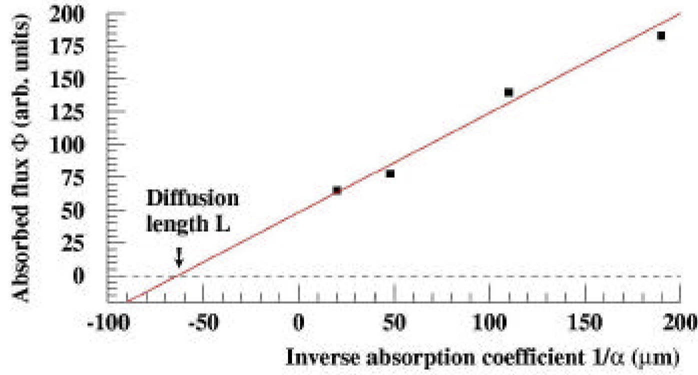

Figure 2.3. Principle of the Surface Photovoltage method.
Squares represent measurement points obtained with different laser wavelengths.

In addition, the SPV method is a steady state measurement in contrast to lifetime measurement techniques based on recording the transient of decaying electron-hole pairs. Such steady state methods are fairly immune against the surface and bulk-trapping effects potentially existing in heavily irradiated silicon [21, and its references]. Clusters of radiation induced defects may provide slow trapping of optically excited charge carriers, which in turn enhance the tail of the decaying transient [13, p. 493], and the obtained value for charge carrier lifetime may be too high.

Another important feature of the SPV method for characterising the effects of radiation damage is that the optical excitation is of relatively low intensity. Therefore, during the measurement, the charge carrier injection level in high resistivity silicon, commonly used in the detector applications, remains low or moderate. Thus, the lifetime of the charge carriers is mainly dependent on the lifetime of the minority charge carriers, and the Schockley-Read-Hall recombination statistic is applicable. This is beneficial since the silicon material quality parameters can generally be extracted only when the effect of minority and majority charge carriers can be separated. Thus, the relationship between the minority carrier lifetime and the trap concentration can be extracted [15]:

$$\boldsymbol{t}_{n,p} = \frac{1}{\boldsymbol{s}_{n,p} v_{th} N_T}, \tag{2.10}$$

where $\boldsymbol{t}_{n,p}$ is the minority carrier lifetime. The term $\boldsymbol{s}_{n,p}$ is the capture cross section of a certain trap level, $\boldsymbol{n}_{th}$ the thermal velocity and N_T the trap concentration. The sub-indexes n and p refer to electrons and holes, respectively.

The leakage current of a reverse biased detector is generation current J_{gen}, which is inversely proportional to generation lifetime, as given in Eq. (2.4). The relation between the recombination and generation lifetimes is given in Eq. (2.6), and in the case of symmetrical charge carrier capture for electrons and holes in Eq. (2.7).

There is well-known square root dependence between the diffusion length and recombination lifetime

$$L = \sqrt{\tau_r D_{n,p}} \tag{2.11}$$

Thus, Eq. (2.4) becomes:

$$J_{Gen} = \frac{qn_i W D_{n,p}}{2L^2 \sqrt{\frac{c_p}{c_n}} \cosh\left(\left(\frac{E_T - E_i}{kT}\right) + 0{,}5 \ln\left(\frac{c_n}{c_p}\right)\right)} \approx \frac{qn_i W D_{n,p}}{L^2 e^{\left(\frac{E_T - E_i}{kT}\right)}} \tag{2.12}$$

In other words, the reverse current is inversely proportional to the square root of the diffusion length:

$$J_{Gen} \propto \frac{1}{L^2} \tag{2.13}$$

2.5 Detection properties using a Silicon Beam Telescope

Helsinki Institute of Physics operates a Silicon Beam Telescope (SiBT) at the CERN H2 test beam [22,23]. The telescope is used to measure tracks of incoming particle beams with high-resolution. SiBT is based on position sensitive silicon detectors attached to readout electronics and data acquisition system. SiBT is an excellent tool for testing the properties of completed particle detectors in LHC-like conditions. With SiBT important detector parameters such as resolution, efficiency, and signal-to-noise ratio can be extracted. The 2002 SiBT layout is shown in Fig. 2.4.

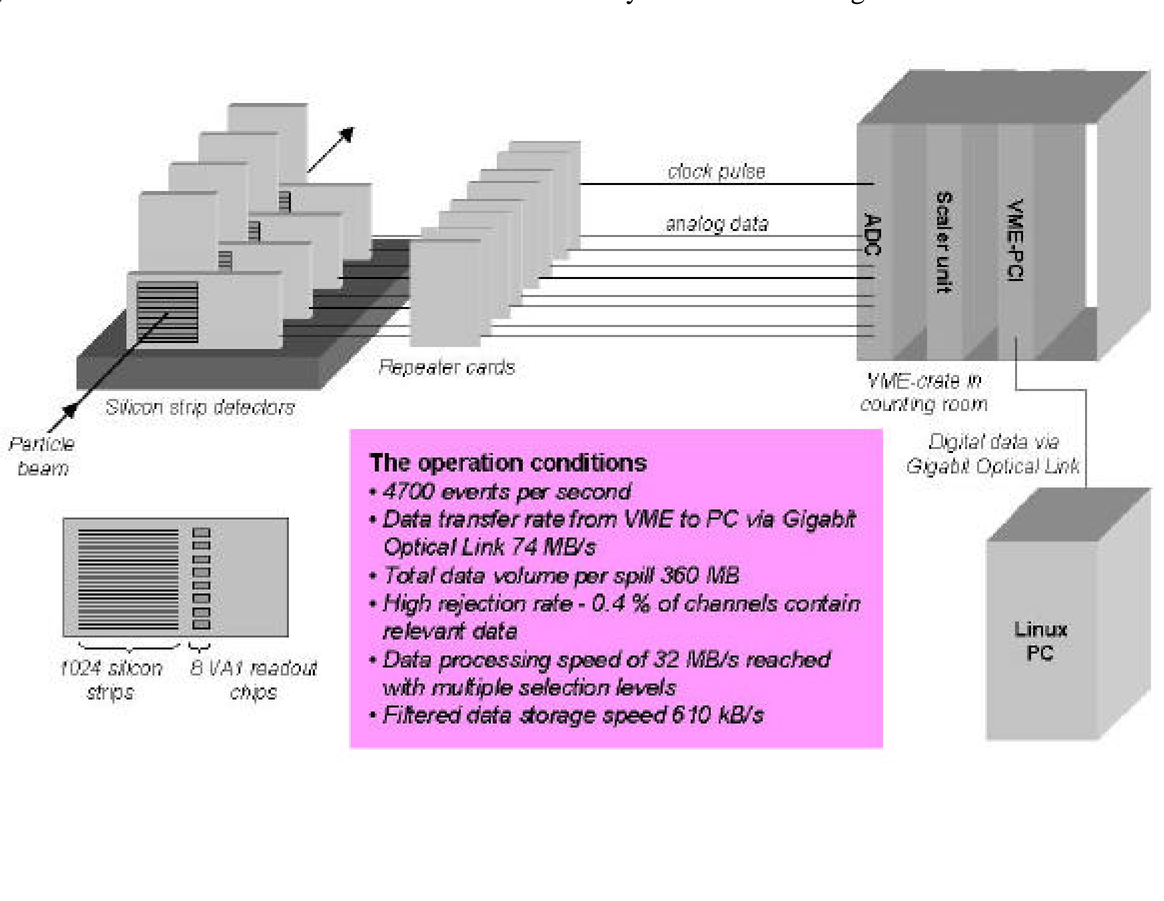

Figure 2.4. Schematics of the HIP Silicon Beam Telescope (picture: Lauri Wendland).

During the summer 2001 SiBT beam tests, an independent Data Acquisition system (DAQ) was installed in a PC. Additionally, new front-end cards were designed and built. During summer 2002, the Data Acquisition was further developed based on a commercial analogue-to-digital converter (ADC) module.

Incoming particle beam

The H2 test beam line that houses the SiBT is derived from a primary proton beam from the CERN SPS (Super Proton Synclotron) accelerator. The protons from SPS have an energy of E = 450 GeV and the extraction cycle length, i.e. the cycle of the spills of particles, of 14.4 seconds. During our measurements the intensity of the primary proton beam was typically $4*10^{11}$ protons per spill. The primary beam of protons hits the so-called T2 primary target and a secondary beam composed of electrons, muons, hadrons, or heavy ions can be extracted. In our experiment, the energy of the chosen muon beam was typically 225 GeV. The beam intensity varied from 200 to 2000 muons per spill.

Silicon detectors

The incoming particle beam passes through four pairs of Silicon strip detectors, ionising charge carriers on its way. Every pair consists of one detector with strips positioned horizontally and another with strips positioned vertically. The single sided detectors have been processed on high resistivity Float Zone silicon (Fz-Si) wafers. The detectors were processed at VTT Electronics in 1996. In this design, two guard rings surround the active areas, and a 3 μm wide floating intermediate strip is located between the read-out strips. The width of the read-out strip is 14 μm, and the distance between the two read-out strips is 55 μm. The area of a detector is 5.6 * 5.6 cm^2, and each detector has 1024 read-out strips. The resistivity of the silicon substrate was chosen so that the 300 μm thick silicon wafer was fully depleted at about 40 V.

The events are triggered by two scintillator detectors, placed before the first detector and after the last detector with respect to the direction of the incoming muon beam. The data readout cycle is started only when an incoming muon hits both scintillators within a set time.

Front-end electronics

Each silicon detector has a separate front-end electronics unit consisting of eight daisy-chained VA1 readout chips glued onto a hybrid board, as well as a front-end card or a repeater card. The VA1 chips are manufactured by the Norwegian company IDEAS. Each VA1 chip has 128 identical channels with a charge-sensitive amplifier, a shaper, and a track-and-hold circuitry in each. The outputs are multiplexed and can be activated by the output shift register using a clock signal. The silicon detector is glued onto a hybrid board with the readout chips, and the 1024 detector readout strips are bonded to the chips, see Fig. 2.5 for a silicon detector glued onto a hybrid board. A 50-pin flat cable connector serves to supply and control the detector via the repeater card.

SiBT repeater cards were reconstructed for the summer 2001 beam tests. Each repeater card contains four voltage regulators to supply the readout chips, and a high-speed differential I/O amplifier to buffer and amplify the balanced analogue output signal. Line receivers and analogue and digital circuits control the readout electronics and set the necessary working parameters for both the detector and the VA1 chips. In addition, the repeater card has an efficient part to protect the readout chips against breakdown damage in latch-up condition. This monitors continuously the input power lines and, if one of them fails to work, cuts off sharply all the supply voltages.

The data readout cycle is started by an external trigger signal that activates the readout modules and starts the readout sequence simultaneously from each of the eight detectors.

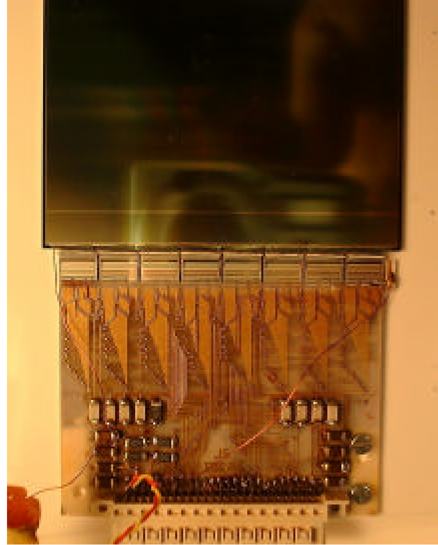

Figure 2.5. Silicon detector glued onto a hybrid board with eight readout chips.

Data Acquisition

A commercial ADC VME module collects the analogue data from the detectors, converts it into digital form, corrects it for pedestal and common mode, and runs the noise suppression and cluster finding algorithms. See Fig. 2.6 for the electronics needed for the SiBT Trigger and Data Acquisition.

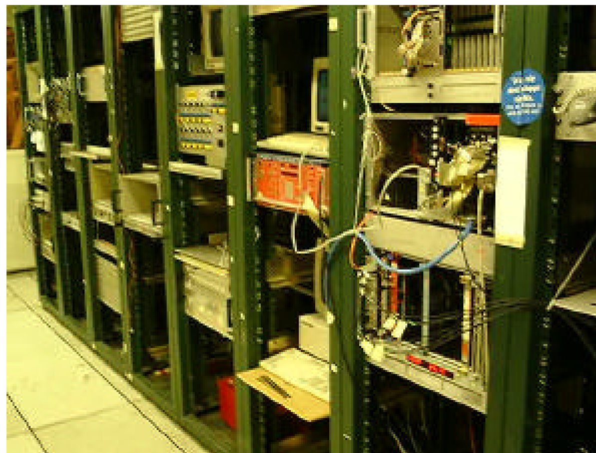

Figure 2.6. SiBT Data Acquisition Electronics.

The PC-based DAQ software sends the data-ready signals to the triggering system during the spill and reads, processes and stores the acquired data once the spill is over. This is realised with a Linux-based C++ code using object-oriented techniques. The DAQ software communicates with the readout system via a PCI-VME interface. Communication with the triggering system is handled through a programmable 16-bit input-output register. The DAQ software also provides minimal, but valuable, online monitoring statistics by calculating the detector efficiencies, the size of the data, and the number of events read.

On-line analysis

To overcome the information gap between the detector hardware and the off-line analysis, an online monitoring program was developed for the SiBT to provide fast feedback of the data to tune the detector hardware and to monitor the quality of the taken data. The online monitoring software does not perform track fitting, but instead it provides all the information of the cluster data and is thus fast enough to provide information of the detector status in real-time. The software is realised with object-oriented techniques using the C++ language, and is thus modular and easily maintainable.

The graphical user interface of the monitoring software was accomplished with a Qt/X11 toolkit [24]. The data received by the online monitoring is visualised by using the Histo-Scope 4.0 histogramming package developed by Fermilab [25]. Histo-Scope enables high interactivity to view the data and because it has a light and modular structure, it is well suited for an online application.

The online monitoring proved to be highly necessary during the test-beam period. It provided valuable information about the performance of the detectors and helped to pinpoint problems and to optimise the noise thresholds of the readout clusterization algorithm during the tuning phase of the hardware. During the data-taking phase, the online monitoring software was used to monitor the quality of the data for possible hardware malfunctions.

Off-line analysis

The off-line analysis of the collected data was performed with an object-oriented software package together with an automatic alignment method. Signal and cluster properties of each detector were studied and plotted. Track reconstruction is performed requiring at least seven hits on a track. Our colleagues from the HIP CMS Theory and Software project did the off-line analysis for the research group, and thus it is outside the scope of this report.

2.6 Irradiations

Proton irradiations were performed at the University of Jyväskylä Accelerator Laboratory. The samples were placed inside a vacuum chamber at the end of the RADiation Effects Facility (RADEF) beam line [26]. The temperature of the diodes was kept below -10°C during the proton irradiation. The protons were passed through a diffusion gold foil, placed 3 meters in front of the chamber, in order to obtain a homogeneous beam of protons throughout the irradiated sample. The beam was collimated 3 cm upstream from the sample, so that the intensity of the proton beam was typically 13 nA/cm^2. The current was monitored on-line using a Faraday cup at the end of the beam line, which could be directly converted into accumulated proton irradiation dose.

During our studies, we performed three sets of detector irradiations at Jyväskylä, with proton energies of 15 MeV, 20 MeV, and 30 Mev.

3 Effect of oxygenation on the radiation hardness of Float Zone silicon

Elevated oxygen concentration in the silicon material is proved to improve the radiation hardness of silicon detectors [4]. The effect of oxygenation has been widely studied by the CERN RD48 (ROSE) Collaboration [27]. However, the influence of oxygenation on the leakage current of irradiated silicon samples has not been reported. At the beginning of our research, we studied the effect of diffusion oxygenation on the radiation hardness of Float Zone silicon. Only later did appropriate material become available so that we could extend our study to Czochralski Silicon, which intrinsically contains high levels of oxygen.

In order to study the properties of the radiation hardness of diffusion oxygenated silicon, we manufactured samples on oxygenated Float Zone silicon (DOF) as well as on standard Float Zone silicon (Fz-Si) for reference purposes. Silicon wafers with two different resistivities were used as starting material. Later, the samples were irradiated with 15 MeV protons using different irradiation doses. The evolvement of the reverse bias current and the minority carrier diffusion length as a function of the dose were measured, and the properties of the radiation tolerance from DOF and Fz-Si were compared. Finally, the long-term stability of the irradiated diodes was studied. The Surface Photovoltage (SPV) method was applied to determine the diffusion length.

3.1 Sample processing and irradiations

Two kinds of 4” n-type Float Zone silicon wafers were used as starting material. Some of the wafers were first oxygenated using dry thermal oxidation followed by a 75-hour drive-in heat treatment at $1050^{o}C$ inert nitrogen gas atmosphere. The oxygen concentration in silicon is estimated to saturate to the value of 10^{17} atoms/cm^2 [27, p. 312]. After the heat treatment, the oxide layer was etched from the wafer surface. The resulting four different materials compared in this study are summarised in Table 3.1.

Table 3.1. Substrate materials used in the study of diffusion oxygenated silicon.

Material	Manufacturer	Resistivity	Thickness	Diffusion oxygenation
Wacker standard	Wacker	> 5 kohmcm	300 ± 20 μm	NO
Topsil standard	Topsil	2 – 3 kohmcm	500 ± 20 μm	NO
Wacker DOF	Wacker	> 5 kohmcm	300 ± 20 μm	YES
Topsil DOF	Topsil	2 – 3 kohmcm	500 ± 20 μm	YES

Some of the four kinds of wafers presented in Table 1 were passivated by thin thermally grown silicon dioxide and then cut into pieces. Small rectangular 0.1225 cm^2 pin-diodes were processed on other wafers. The diodes were processed as explained in Chapter 2.1.

Pin-diodes and pieces of passivated wafers were irradiated with 15 MeV protons at Jyväskylä University Accelerator Laboratory as described in Chapter 2.6. Three different irradiation doses were used: $6.0*10^{12}$, $5.0*10^{13}$, and $1.0*10^{14}$ protons/cm^2. Some samples were left as reference without irradiation. Proton irradiation doses can be expressed as an equivalent dose of 1 MeV neutrons: $2.0*10^{13}$, $1.7*10^{14}$, and $3.3*10^{14}$ neutrons/cm^2, respectively, calculated according to ref. [28]. In comparison, a total dose of $1.6*10^{14}$ cm^{-2} 1 MeV neutrons/cm^2 is predicted for the inner parts of CMS after 10 years of operation [29].

3.2 Effect of oxygenation on the diffusion length of silicon

Minority carrier diffusion lengths were measured from the irradiated samples using the SPV method, as described in Chapter 3.4. Initial diffusion lengths, i.e. values for non-irradiated samples, could not be measured by SPV since this method is applicable only when the diffusion length is shorter than the thickness of the silicon sample [15], which is not the case with high-purity silicon material.

The pre-irradiation diffusion lengths were calculated by Eq. (2.11) from the lifetime values measured by μPCD method. The principle of the PCD measurement is described in detail in Ref. [13] and its application for the characterisation of particle detectors in Chapter 2.3. The diffusion constant for holes, D_p, was assumed to be 12 cm^2/s.

The results of SPV measurements are presented in Fig. 3.1. Each data point is an average value of at least ten SPV measurements. The standard deviation of the diffusion length was found to be negligible in the irradiated areas. The post-irradiation diffusion lengths in Fig. 3.1 are normalised to the pre-irradiation values. In the diffusion oxygenated silicon samples, the values of pre-irradiation diffusion lengths were practically same before and after oxidation.

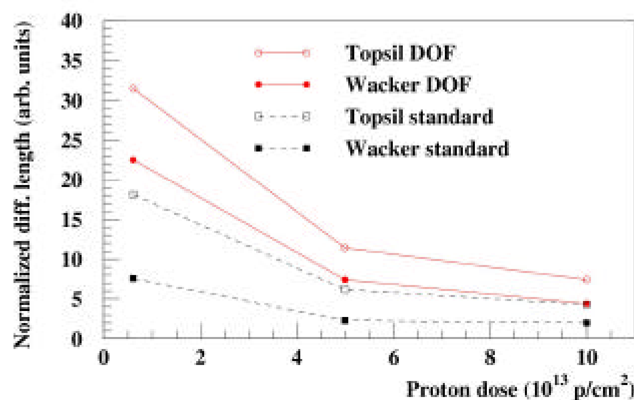

Figure 3.1. Normalised minority carrier diffusion lengths as a function of irradiation dose with 15 MeV protons.

As expected, the diffusion length decreases as the irradiation dose increases. The diffusion lengths in the material of lower resistivity (i.e. Topsil) are consistently higher than those in the material of higher initial resistivity (i.e. Wacker). This phenomenon is supposedly related to microscopic properties of the two different silicon materials. However, in this study we used too few different materials to draw conclusions about the reasons for the phenomenon.

As clearly seen in Fig. 3.1, oxygenation of silicon improves the minority carrier diffusion lengths in irradiated silicon material. In the oxygenated silicon samples, the degradation of diffusion length during the irradiation was smaller. The positive effect of oxygenation for increasing the diffusion length is noticeable in the case of both lower and higher resistivity silicon.

Additionally, the beneficial effect of oxygenation seems to diminish at higher proton doses. This phenomenon might be caused by the increasing number of radiation-induced defect states compared to the number of originally introduced oxygen states, thus decreasing the beneficial effect of oxygenation.

3.3 Effect of oxygenation on the leakage current of silicon

Leakage current in a silicon device is generation current caused by generation-recombination centres, i.e. impurities or defects. Thus, leakage current depends on recombination lifetime, as explained in Ref. [15]. Lifetime and diffusion length are related according to Eq. (2.11).

Furthermore, in order to study the effect of oxygenation on the leakage current of silicon, diode current-voltage characteristics was measured after different irradiation doses. Leakage currents were measured after 10 hours of annealing at 80°C. The temperature during the measurement was 24°C, and the relative humidity 43 %. Diode guard rings were grounded. The results are shown in Fig. 3.2.

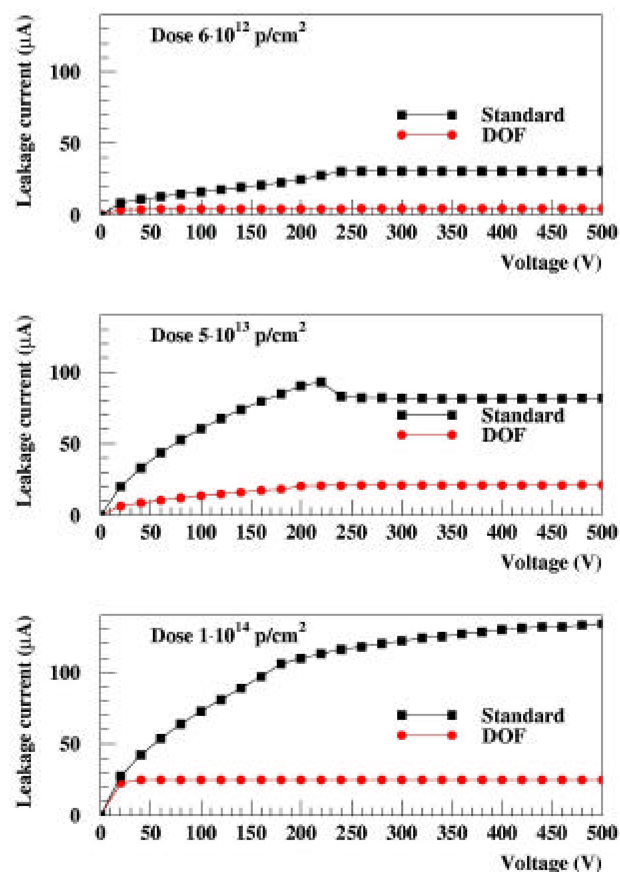

Figure 3.2. Diode current-voltage characteristics of oxygenated and non-oxygenated silicon samples measured after irradiations by different doses.

As shown in Fig. 3.2, diffusion oxygenation of the silicon material clearly improves the leakage current properties of irradiated silicon. This effect is obvious for every irradiation dose. Until now, the influence of oxygenation on the leakage current of irradiated silicon samples has not been reported.

In the standard silicon, there is a jolt in the leakage current curve around the depletion voltage (200 V). This might be connected to the current through the detector guard ring.

3.4 Suitability of SPV for characterising irradiated silicon

In order to verify the accuracy of the SPV method for studying irradiated silicon samples, the diffusion lengths measured using SPV were used as starting values for simulating diode current-voltage curves by one-dimensional PC1D-software [30]. Other essential simulation parameters were the process values used during the sample fabrication, as well as simulated junction depths, as presented in Chapter 2.1. The scrutinised diodes were made of non-oxygenated silicon manufactured by Topsil, irradiated with a total dose of $5*10^{13}$ protons/cm^2. Simulated and measured IV-curves are shown in Fig. 3.3. The measured IV curve is an average value of seven diodes.

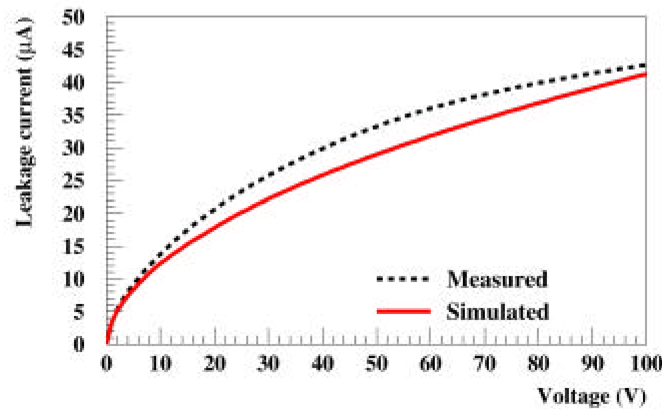

Figure 3.3. Measured and simulated IV-curves of Topsil standard diodes irradiated with $5.0*10^{13}$ protons/cm^2, i.e. a dose equal to approximately 10 years of LHC operation.

As seen in Fig. 3.3, there is a good agreement between simulated and measured current-voltage values. Additionally, similar consistency was found with both Wacker and Topsil diodes irradiated with different doses. A small discrepancy between the simulated and measured values is expected as computer simulations are always based on ideal models. In addition, the simulation was done one-dimensionally. Further simulations confirmed that the reverse leakage current is insensitive to surface effects including surface recombination velocity and positive oxide charge induced by radiation defects. Thus, the radiation-induced defects are undoubtedly the dominant contributors to generation current.

The suitability of the SPV method for characterising irradiated silicon samples was proved. The SPV method is a practical method for characterising irradiated silicon samples. Particle radiation degrades both the surface and the bulk properties of silicon. Unlike in other lifetime measurement methods, in SPV measurement the surface effects can be excluded and an unambiguous value for the bulk lifetime can be obtained. In addition, the SPV method is a steady state measurement and is thus fairly immune to the trapping effects of optically excited charge carriers potentially existing in heavily irradiated silicon. Because of trapping effects, the obtained value for charge carrier lifetime may be too high. Another important feature of the SPV method is that the optical excitation is of relatively low intensity. Consequently, the effects of minority and majority charge carriers can be separated.

3.5 Effect of oxygenation on the long term stability of irradiated silicon

The electrical activity of radiation-induced defects is known to change according to time and temperature [1]. This is understandable, since in the silicon material the migration of defects, e.g. vacancies and interstitials, obey exponential laws with such variables as activation energy and

temperature. In order to speed up the defect reactions after the exposure to particle radiation, silicon samples are heat treated at elevated temperatures. In this way, the long-term stability of silicon detectors in hostile radiation environment can be studied. Additionally, information about the origin of the defects can be revealed.

We did an annealing study to compare the properties of oxygenated and non-oxygenated silicon diodes. The irradiated silicon diodes were annealed at a temperature of 80°C up to ten hours. According to Ref. [31, p. 3], one minute of heat treatment at 80°C corresponds several years in the CMS inner detector that is operated at -10°C as well as about 100 hours at room temperature (20°C), present during the LHC maintenance breaks. Between each heat treatment step, reverse current and minority carrier diffusion length were measured from the samples. Surface Photovoltage (SPV) method was used to determine the diffusion length. Between the heat treatments and measurements, the samples were stored refrigerated at well below 0°C.

The effect of annealing on diffusion length

The time evolution of the diffusion length during the annealing process is presented in Figs. 3.4a, 3.4b, and 3.4c after the high, medium, and low irradiation dose, respectively. In each figure, the results from all the four different kinds of silicon material are shown, i.e. Topsil standard, Topsil DOF, Wacker standard, and Wacker DOF, as presented in Table 3.1.

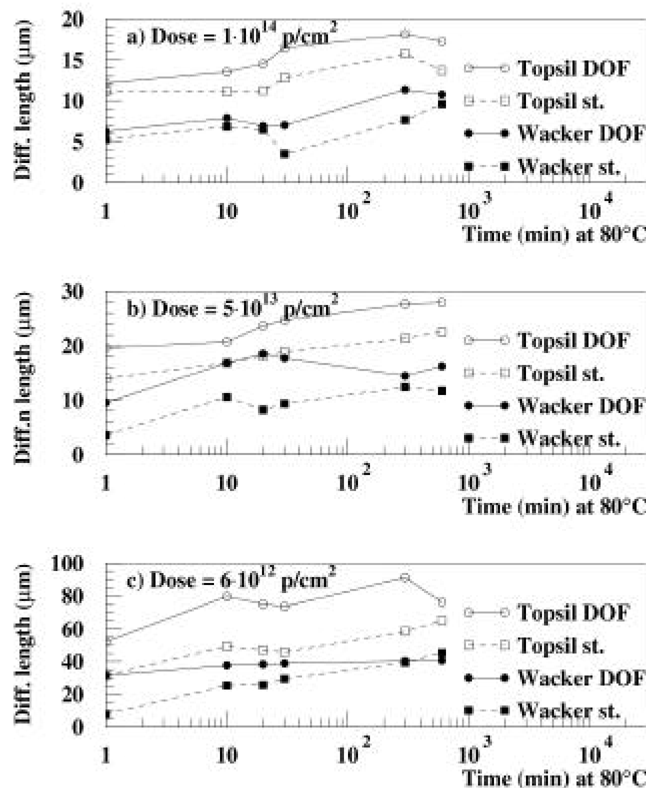

Figure 3.4. Diffusion length as a function of annealing time at 80°C after a) high irradiation dose, b) medium irradiation dose, and c) low irradiation dose. Each diffusion length value is an average of ten measurement points in the middle of the irradiated silicon sample.

As seen in Fig. 3.4, significant improvement in the diffusion lengths can be noticed after the first annealing steps regardless of the sample resistivity or the oxygen concentration. The improvement is noticeable during the first 30 minutes, but later the improvement slows down. In the higher resistivity silicon material, irradiated with medium and high doses, a drop in the diffusion length was observed both in oxygenated and non-oxygenated samples after 30 minutes of annealing. However, in the oxygenated material, the drop was much smaller, i.e. the oxygenated material was more stable. This phenomenon was not seen in the lower resistivity silicon material.

The effect of annealing on reverse current

The time evolution of the reverse current values during the annealing is presented in Figs. 3.5a and 3.5b for diodes made of oxygenated and non-oxygenated silicon from Topsil. As seen in Fig. 3.5a, peculiar behaviour was observed in the samples made of the non-oxygenated higher resistivity material and irradiated with high and medium doses. Sudden drops in the reverse current values were observed. Furthermore, in the same sample, the diode-like behaviour disappeared after the irradiation by the lowest dose, but reappeared after annealing. This instability in the diode characteristics was not observed in either of the oxygenated materials.

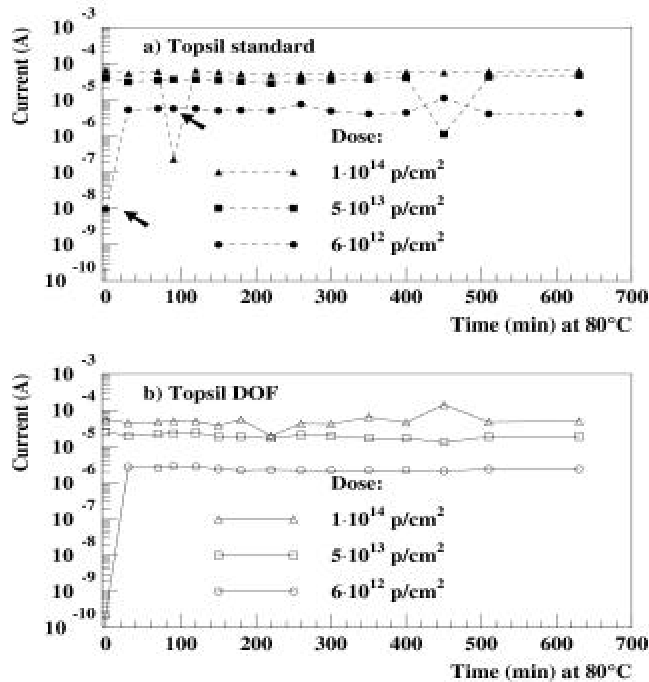

Figure 3.5. Reverse current at 100 V as a function of the annealing time at 80°C measured from a) non-oxygenated Topsil standard diodes and b) oxygenated Topsil DOF diodes.

Thus, this annealing study demonstrated that diffusion oxygenation reduces the instability in irradiated silicon, seen both in diffusion length and reverse current measurements. The explanation of the origin of the instability is outside the scope of this report. It is, however, obvious that the instability is linked with the kinetics of the radiation induced defects. The behaviour of the diffusion length as a function of the annealing time is similar to that reported in systematic studies where the effective doping concentration is monitored [31].

Reliability of the SPV method

Additionally, we studied the accuracy of the SPV method. Measured leakage currents and the respective values of diffusion lengths measured by SPV are presented in Fig. 3.6. Exponential curve, $y = kx^n$, is fitted to the experimental data points, and the value of n is –1,9599. Thus, the reverse current is inversely proportional to the square of the diffusion length. This is the relationship deduced previously and shown in Eq. (2.13). Therefore, the SPV method gives a reliable value for the diffusion length, which in turn allows us estimate the reverse current. In other words, the SPV method proved to be a reliable characterisation method for irradiated silicon samples.

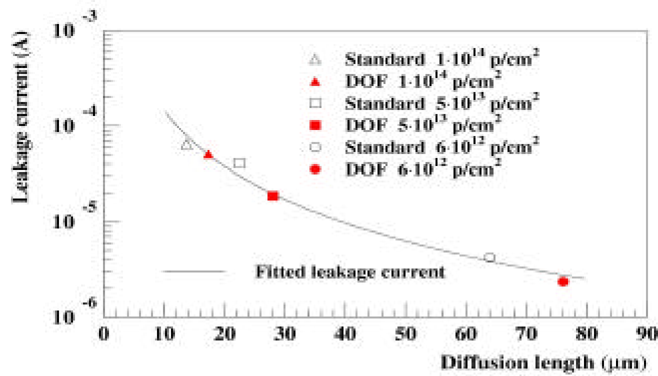

Figure 3.6. Reverse current as a function of diffusion length.
Data points correspond to measured values after 10 hours of annealing.

4 Czochralski silicon as material for radiation hard particle detectors

At the beginning of 2002, we received high resistivity Czochralski silicon (Cz-Si) wafers from Finnish manufacturer Okmetic Oyj. Several other groups have studied Czochralski silicon as detector material, but because of the lack of availability of high resistivity Cz-Si wafers, this was the first time full-size Cz-Si detectors were manufactured, characterised, tested in a particle beam, and irradiated.

In order to study the properties of the radiation hardness of Czochralski silicon, we processed large area strip detectors and test structures on Czochralski silicon (Cz-Si), as well as on oxygenated Float Zone silicon (DOF) and standard Float Zone silicon (Fz-Si) for reference purposes. Minority carrier lifetimes were characterised using the Photoconductive Decay (PCD) method, and defect states were characterised by Deep Level Transient Spectroscopy (DLTS) measurements. Current-Voltage (IV) and Capacitance-Voltage (CV) measurements were used to measure detector parameters. Then, the properties of the detectors were tested in a particle beam. Later, the samples were irradiated with 10 and 20 MeV protons using different irradiation doses. The evolvement of the reverse bias current and the minority carrier diffusion length as a function of the dose were measured and the properties of the radiation tolerance from Cz-Si, DOF and Fz-Si were compared.

4.1 Why high resistivity Czochralski silicon?

Silicon detectors have traditionally been processed using Float Zone silicon (Fz-Si) wafers. Fz-Si crystals are grown without quartz crucibles acting as a source of impurities, i.e. oxygen, carbon, or boron. The lack of impurities results in high purity and high resistivity of the bulk silicon. Because of the high resistivity, the detector can be fully depleted at reasonable operating voltages. However, Fz-Si has a low oxygen concentration. The oxygen concentration can be increased by prolonged high temperature drive-in oxygen diffusion. Unfortunately, some metallic contamination is always present in quartz tube diffusion furnaces. At elevated temperatures, the diffusion velocity of many harmful metals is much higher than that of oxygen. This in turn may lead to an extensive process induced contamination in the silicon wafers, unless a careful quartz tube cleaning procedure is practised.

Silicon wafers grown using the Czochralski method intrinsically contain high level of oxygen, typically 10^{17} – 10^{18} cm^{-3}. In addition, the depletion voltage of the Czochralski silicon (Cz-Si) detectors can be tailored either by adjusting the oxygen concentration in the silicon bulk during crystal growth or by manipulating the thermal history of wafers during the detector processing.

Furthermore, using Cz-Si as detector material may offer economical benefits. Cz-Si wafers are available up to a diameter of 300 mm while Fz-Si wafers are typically of diameter 100 mm or 150 mm. Thus, very large area silicon detectors could be manufactured, which in turn could result in significant savings in the costs related to front-end electronics, interconnection, and module assembly.

In spite of the obvious advantages, this is the first time large area Cz-Si detectors have been manufactured and tested. This is due to the lack of availability of high resistivity Cz-Si wafers. Cz-Si is a basic material for the microelectronics industry, but only recently has there been demand and availability of high resistivity Cz-Si material. However, resistivities up to 5 kΩcm have been reported, both in p-and n-type silicon [32].

4.2 Crystal growth of Czochralski silicon

In the Czochralski method, polycrystalline silicon fragments are melted inside a quartz crucible. During the process, argon gas continuously flushes the interior of the crucible and the surface of the silicon melt. Silicon single crystals are grown by slowly pulling a crystal seed up from the molten silicon, thus developing an ingot. Later, wafers are cut from the ingot.

Oxygen concentration is one of the most important parameters of silicon wafers. For example, oxygen precipitates bind unwanted metallic impurities present during the processing of silicon devices [33,34]. Furthermore, stress induced during high temperature processing can lead to the formation of slip defects in the wafer. The presence of oxygen stabilises the wafer, and thus Cz-Si wafers are less prone to slip than Fz-Si wafers [35].

During crystal growth, oxygen is dissolved into silicon from the quartz crucible. Most of the oxygen is dissolved as silicon monoxide and is flushed away by argon gas. Furthermore, the resulting oxygen concentration depends on the velocity of the silicon melt flow as well as on the rate of oxygen evaporation from the surface of the melt. All these parameters can be influenced in order to get a desired oxygen concentration in silicon ingot. Since the silicon melt is an electrically conductive liquid, the magnetic field is an effective way to moderate and control the melt flow. The Magnetic Czochralski (MCZ) method has several advantages, e.g. reducing the erosion of the silica crucible and thus reducing introduction of impurities during crystal growth [36].

In order to grow n-type silicon ingots, phosphorous dopant is added to the silicon melt in order to create desired donor states in silicon. However, boron is a common element in nature and thus easily drifts from quartz crucible to silicon melt during crystal growth. Since boron acts as an acceptor in silicon, the amount of unwanted boron is an important limitation to the magnitude of resistivity in n-type silicon [37].

4.3 Processing Czochralski silicon detectors

We processed large area strip detectors on silicon wafers grown using the magnetic Czochralski (MCZ) method. The phosphorous-doped n-type <100> Cz-Si wafers manufactured by Okmetic Oyj have a nominal resistivity of about 900 Ωcm. The wafers are single side polished with a thickness of 380 μm. The oxygen concentration of the material is less than 10 ppma (parts per million atomaric). This concentration is an order of magnitude larger than is realisable by drive-in diffusion oxygenation [14, p. 69], but slightly less than in the Cz-Si wafers typically used in the microelectronics.

The relatively low oxygen concentration in the wafers is due to the use of magnetic field, which during crystal growth is used to control the amount of oxygen dissolving from the silica crucible into the silicon bulk [36]. The low oxygen concentration is favourable in order to avoid unwanted oxygen precipitation in the high temperature treatments during detector processing.

The detectors were processed at the Helsinki University of Technology Microelectronics Centre. Our detector fabrication process is very simple, containing four lithography levels, two thermal oxidations, two ion implantations, and three sputter depositions. The size of the AC-coupled detector is 32.5 cm^2.

The width of each of the 1024 p^+-strip implants is 10 µm, the length is 6,154 cm, and the strip pitch is 50 µm. The coupling insulator above each strip is a 200 nm thick silicon dioxide film grown using thermal dry oxidation. Each strip is connected to the common bias line via a bias resistor. Five guard rings surround the active area of the detector. In addition, test structures were processed on the edges of the wafer. For reference purposes, Fz-Si (Topsil AS) standard and diffusion oxygenated detectors were processed simultaneously using single-side-polished 520 µm-thick wafers with resistivity of about 3 kΩcm. The fabrication process is described in detail in Chapter 2.1.

4.4 Lifetime of minority charge carriers

Minority carrier lifetimes were measured using the µPCD method from oxidised wafers, as described in Chapter 2.3. The PCD measurement is made in less than one second per measurement point, typically of the area 1 mm^2. As a result, the lifetimes from the whole silicon wafer can be mapped in a reasonably short time. A lifetime measurement from a Czochralski silicon (Cz-Si) wafer is shown in Fig. 4.1a, and a measurement of a standard Float Zone silicon (Fz-Si) reference wafer is shown in Fig. 4.1b.

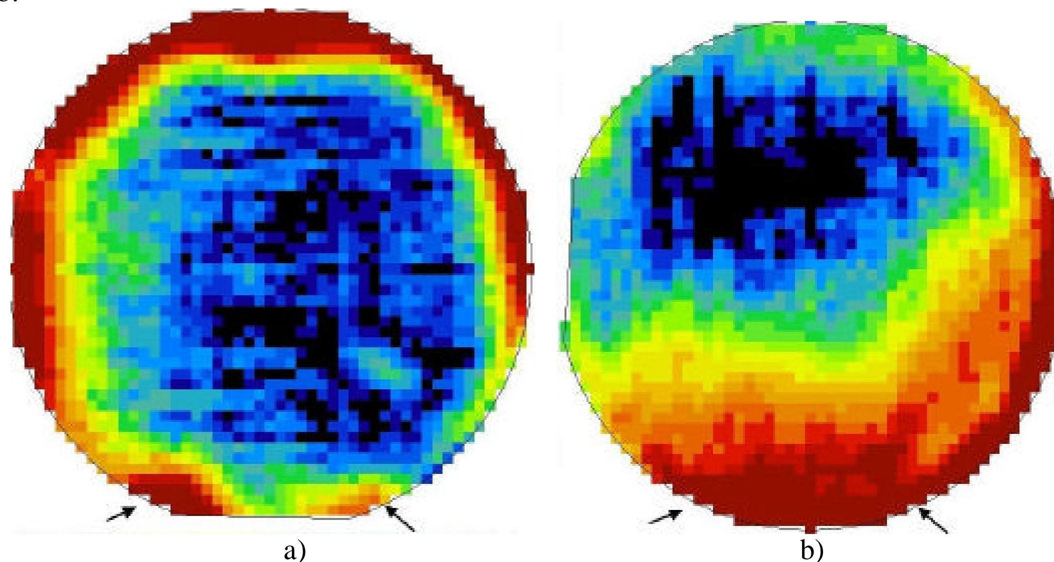

Figure 4.1. Lifetime maps of a) Okmetic Czochralski silicon wafer and b) Topsil Float Zone silicon wafer. Both wafers are thermally dry oxidised before measurement. The arrows point at the areas that are contaminated by the quartz boats of the oxidation furnace. Measured values of the lifetime are a) from 250 us (on the edges) to about 4000 us (in the centre) and b) from 650 us (on the edges) to about 4000 us (in the centre).

In Cz-Si wafers, the beneficial effect of oxygen could clearly be seen in the lifetime maps of Fig. 4.1. In Cz-Si wafers, the contamination pattern is circularly symmetric, i.e. the region of lower lifetime was reduced to the edges of the wafer. On the other hand, in the Fz-Si wafers, a typical quartz boat contamination can be seen, i.e. metals (e.g. iron and alkaline metals) diffusing from the touching quartz parts into the wafer and further diffusion from this area towards the centre of the wafer. It is worth mentioning that the Cz-Si and Fz-Si wafers shown in Figs. 4.1a and 4.1b, respectively, were oxidised simultaneously in the same quartz boat in a dry O_2 atmosphere for eight hours at 1050°C.

Obviously, in the case of Cz-Si wafers, the metallic impurities originating from the quartz parts of the diffusion furnace are relatively effectively gettered into the oxygen precipitations present in the Cz-Si material. The essential difference between the silicon wafers grown by Czochralski and Float Zone methods is the concentration of oxygen and carbon. Oxygen in silicon is a widely studied topic. In addition to the assumed improving effect on the radiation hardness of silicon detectors, oxygen as an impurity in silicon crystal has other beneficial properties.

For example, it is well known that oxygen and oxygen precipitates bind metallic impurities, present intrinsically or induced during the processing, which become mobile because of high temperature treatments during the device manufacturing [33,34]. Gettering effects may explain the results shown in Figs. 4.1a and 4.1b. The metallic impurities originating from the quartz parts of the diffusion furnace are relatively effectively gettered into the oxygen precipitations existing in small concentrations in the Cz-Si material. Thus, the charge carrier lifetime remains high throughout the silicon wafer, as seen in Fig. 4.1a. On the other hand, in the Fz-Si material the oxygen concentration is low and the number of preferential gettering sites is small. Thus, the metallic contamination can diffuse freely during the high temperature processing, resulting in a lifetime pattern shown in Fig. 4.1b.

Obviously, the circularly symmetric contamination pattern in the Cz-Si lifetime map shown in Fig. 4.1a is due rather to the conditions of crystal growth than the conditions of wafer oxidation. The purpose of the magnetic field during crystal growth is to allow better control of the flow of liquid silicon melt, which reduces the risk of generation of dislocations, especially in the case of large diameter silicon single crystals. However, the magnetic field might affect the concentration of the gettering oxygen on the wafer edges. Very strong damping induced by a magnetic field decreases the stirring of the silicon melt and the impurities therein, which may result in larger radial variation in oxygen and dopant concentrations in the silicon crystal [36].

4.5 Defect characterisation

In order to study the thermal stability of high-resistivity Cz-Si, DLTS (Deep Level Transient Spectroscopy) [38] measurements were performed on diodes at Ioffe PTI, St. Petersburg. Dr. Elena Verbitskaya carried out both the measurements and the analysis. The measurements were done on p^+-n-n^+ diodes using C-DLTS technique either with injection of electrons only (reverse bias) or electrons and holes (forward bias). The diodes were located near the wafer edges, which are somewhat contaminated, as shown in the lifetime maps of Fig. 4.1. Comparison of experimental deep level spectra for Fz-Si and Cz-Si detectors is presented in Fig. 4.2.

Parameters of deep levels were determined using C-DLTS spectra simulation and a fitting program. The carrier emission from any defect results in the peak defined by three parameters: E_t, the position of the defect level in the band gap with respect to the bands; ***s***, the carrier capture cross-section, and N_t, the concentration of deep level participating in emission / trapping processes.

Two electron traps, E1 (higher peak in Fig. 4.2) and E2 (lower peak in Fig. 4.2), are detected in the spectra of any detector from Cz-Si and Fz-Si as seen in Table 4.1. In both types of silicon the dominant peak is the midgap defect E1, however its concentration N_t in Cz-Si is $1 \cdot 10^{11}$ cm^{-3}, which is three times larger than that in Fz-Si. The difference in the E2 concentration is more essential; its values in Cz-Si and Fz-Si are respectively $5.4 \cdot 10^{10}$ and $3.5 \cdot 10^{9}$ cm^{-3}, respectively, which may be related to the fact that in Fz-Si with a larger resistivity, the Fermi level is located closer to the midgap, and the filling of the E2 energy level positioned at $E_c - 0.27$ eV is hardly disturbed by carrier injection.

The main difference of as-processed defects is observed in DLTS spectra measured with electron/hole injection (Fig. 4.2b). The signal from E1 and E2 is observed in Cz-Si whereas only the hole trap H1 with the energy $E_v + 0.27$ eV is revealed in Fz-Si. This hole trap is also evinced in Cz-Si resulting in the reduced width of the peak originated from E2 trap. The wide peaks in the temperature range of 170 to 250 K in the spectra of Fz-Si with electron/hole injection are too weak, and the parameters of these defects cannot be defined by simulation.

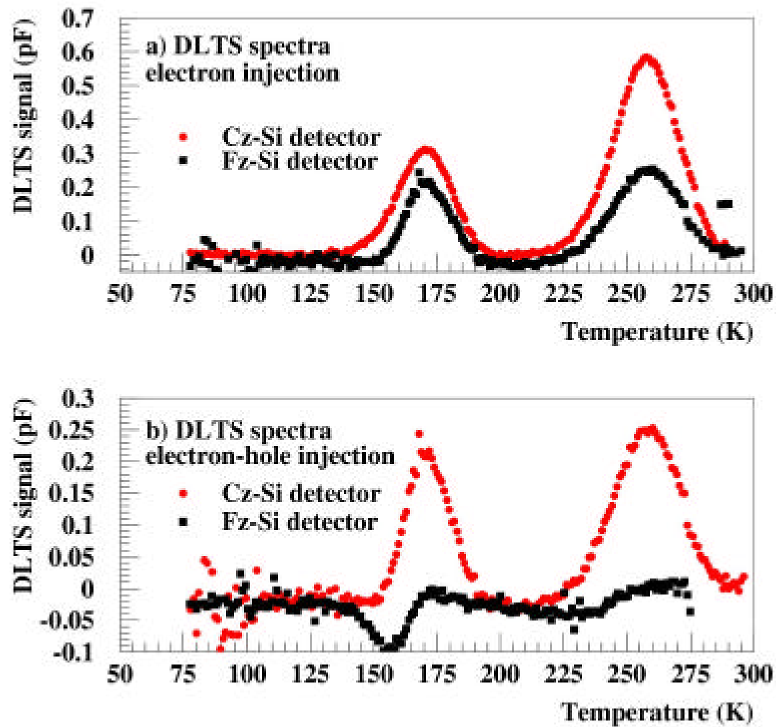

Figure 4.2. Deep level spectra for detectors from Czochralski Silicon (Cz-Si) and Float Zone Silicon (Fz-Si) measured with a) electron and b) electron/hole injection.

For the analysis of the observed levels of thermally induced defects in as-processed detectors from Cz-Si and Fz-Si, the results of Ref. [39] were used. It follows from the comparison of these results that E1 and E2 are specific defects induced by heat treatment into the silicon bulk and usually referred to in the literature as Sah levels [40]. The enlarged concentration of E1 trap revealed in our study in Cz-Si agrees with the results of [39], where the concentration of this midgap defect was higher for the diodes from Cz-Si compared to those from Fz-Si, see Table 4.2.

In conclusion, according to [39], the difference in deep level E1 concentration was caused by the higher temperature of the silicon thermal oxidation and, additionally, to the increased oxygen concentration in Cz-Si. Hence, the Cz-Si shows the specific features of high oxygen concentration compared with the Fz-Si material. On the other hand, since the concentration of E1 defect in Cz-Si ($\sim 1 \cdot 10^{11}$ cm^{-3}) is smaller than that of shallow donors, it cannot change the type of conductivity of the initial silicon. Therefore, this type of silicon is promising for processing the detectors operating in a high radiation environment, and also for regular detectors.

Table 4.1. Parameters of deep levels in as-processed detectors

Material	Sample #	Injection	Type of trap	E_t* (eV)	σ (cm2)	N_t (cm^{-3})
Cz-Si	1	electron	E1	0.56	$5\cdot10^{-15}$	$1\cdot10^{11}$
			E2	0.267	$1\cdot10^{-17}$	$5.4\cdot10^{10}$
		electron/hole	E1	0.56	$5\cdot10^{-15}$	$4.5\cdot10^{10}$
			E2	0.27	$1.5\cdot10^{-17}$	$3.8\cdot10^{10}$
			H1	0.27	$3\cdot10^{-16}$	$1.6\cdot10^{9}$
	2	electron	E1	0.56	$5\cdot10^{-15}$	$1\cdot10^{11}$
			E2	0.27	$1.3\cdot10^{-17}$	$5.45\cdot10^{10}$
		electron/hole	E1	0.56	$1.9\cdot10^{-14}$	$4.5\cdot10^{10}$
			E2	0.27	$1.3\cdot10^{-17}$	$3.8\cdot10^{10}$
			H1	0.27	$4\cdot10^{-16}$	$1\cdot10^{10}$
Fz-Si	1	electron	E1	0.562	$5\cdot10^{-15}$	$3.3\cdot10^{10}$
			E2	0.267	$1.1\cdot10^{-17}$	$3.5\cdot10^{9}$
		electron/hole	E3	0.19	$1\cdot10^{-15}$	$5\cdot10^{9}$
			H1	0.27	$3\cdot10^{-16}$	$1\cdot10^{10}$
	2	electron	E1	0.562	$5\cdot10^{-15}$	$3.4\cdot10^{10}$
			E2	0.27	$1\cdot10^{-17}$	$3.5\cdot10^{9}$
		electron/hole	E3	0.19	$9\cdot10^{-16}$	$5\cdot10^{9}$
			H1	0.27	$3\cdot10^{-16}$	$1.2\cdot10^{10}$

*E_t is the energy gap defined from the E_c bottom and the E_v top for electron and hole traps, respectively.

Table 4.2. Availability of midgap energy levels E1 in as-processed detectors from different types of silicon.

Material	Fz-Si [1]	Cz-Si [1]	Fz-Si [this study]	Cz-Si [this study]
lower T treatment	-	+		
high T treatment	+	+	$3.3\cdot10^{10}$ cm^{-3}	$1\cdot10^{11}$ cm^{-3}

4.6 Detector characterisation

Leakage current

Detector leakage currents were characterised using current-voltage measurements. Detector current-voltage (IV) characteristics up to 900 V were measured using probe stations and adjacent measurement set-ups. Measurements were performed in a clean room at room temperature without dry nitrogen flush to detectors already sawed from wafers. Leakage currents measured from Cz-Si and Fz-Si detectors are presented in Fig. 4.3.

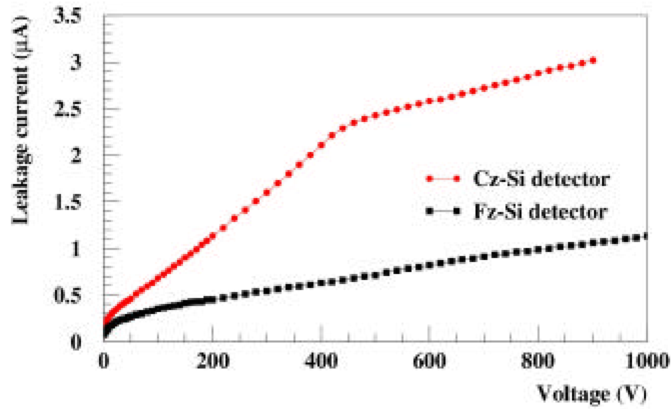

Figure 4.3. Current-voltage characteristics measured from 32.5 cm^2 Cz-Si and Fz-Si detectors.

The leakage current value of 3 µA at 900 V was measured for a 32.5 cm^2 Czochralski silicon detector. No breakdown occurred below 900 V. For comparison, the leakage current in the reference Float Zone silicon detector was 1,2 µA at 1000 V, without breakdown. Indeed, in the CERN CMS experiment, a silicon detector of similar size is considered to belong to the highest quality class when the leakage current does not exceed 4 µA at 450 V [29]. The main contributors to the good breakdown properties are rounded corners in the strips (as seen in Fig. 2.1), deep junctions, and metal overhang over the strip implants [41].

Depletion voltage

Full depletion voltages of Cz-Si and Fz-Si samples were extracted from capacitance-voltage (CV) measurements. The CV measurement was carried out on a 6 mm * 6 mm test diode, located in the edge region of the silicon wafer. The CV-measurement was carried out at the frequency of 100 kHz. The $1/C^2$ plot of the measurement data is shown in Fig. 4.4.

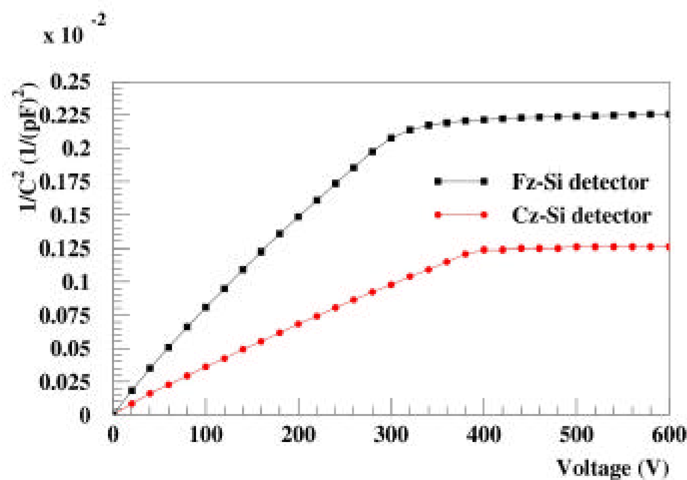

Figure 4.4. Capacitance $1/C^2$ plots from Cz-Si and Fz-Si samples.

Estimation for the depletion voltage of the Cz-Si device can be made from Fig. 4.4. The plateau of the curve starts at about 420 V for the 380 μm thick substrate. For comparison, for the Fz-Si device the depletion occurs at about 320 - 340 V for the 500 μm thick substrate. As measured previously, there is no breakdown around these values.

The doping concentration and resistivity can be calculated from the well-known formula of the full depletion voltage:

$$V_{fd} = \frac{qN_d d^2}{2\varepsilon_0 \varepsilon_{Si}}, \qquad (4.1)$$

where q is the elementary charge, N_d the doping concentration, d the thickness of the substrate, ε_0 the dielectric constant of the vacuum, and ε_{Si} the dielectric constant of the silicon. For a 380 μm thick Cz-Si substrate, the depletion voltage of about 420 V would result in a resistivity of about 1150 Ωcm, which is slightly more than the 900 Ωcm measured before the device processing. If the wafers were thinned down to 300 μm, which is frequently the thickness in the particle detector applications, the resistivity of 1150 Ωcm would cause the detector to be depleted at about 265 V, as calculated from Eq. (4.1).

Generally in device processing, impurities diffuse to silicon during the high temperature heat treatments, thus decreasing the electrical resistivity. However, during our detector process, the electrical resistivity of Cz-Si wafers increased significantly. This was in spite of the fact that we had no specific donor-killing treatment in our process. In addition, the Cz-Si and Fz-Si devices were processed simultaneously in the same diffusion furnace.

4.7 Performance of Czochralski silicon in particle detection

After the electrical characterisation, the particle detection performance of the Cz-Si detector was studied using the Silicon Beam Telescope (SiBT) of the Helsinki Institute of Physics at the CERN H2 test beam [22,23]. The telescope is used to measure tracks of incoming particle beams with high-resolution. The SiBT consists of position sensitive silicon detectors attached to readout electronics and a data acquisition system. A detailed description of SiBT can be found in Chapter 2.5.

The Cz-Si detector proved to perform well as a particle detector. A muon beam of the energy of 225 GeV was used to measure its properties. The important detector parameters, including signal size distributions and signal to noise distributions, were successfully extracted from the Cz-Si detector. The efficiency of the detector was measured to be 95 %, the resolution about 10 um, and the signal to noise ratio about 10. The hit profile and pulse height distribution of the Czochralski detector are shown in Fig. 4.5. The graph includes 10^6 muon events.

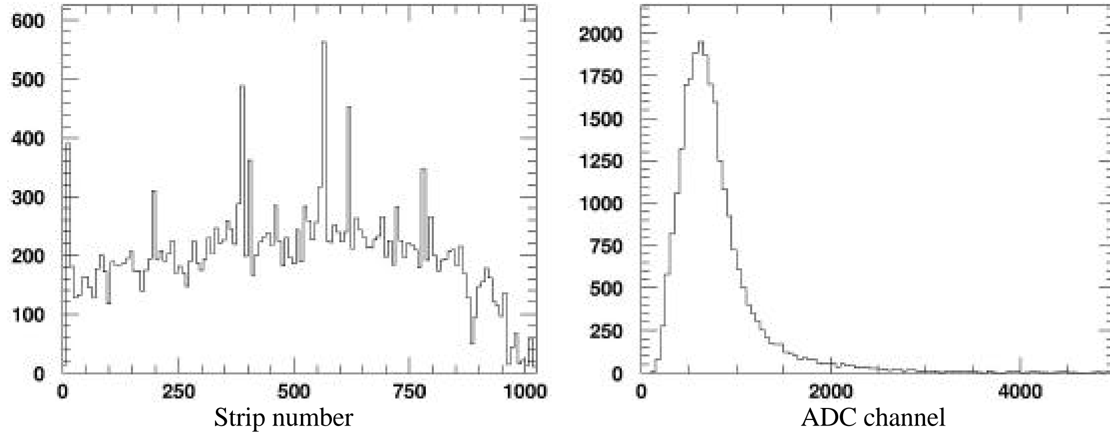

Figure 4.5. Hit profile and pulse height distribution (counts per channel) of the Czochralski detector.

4.8 Irradiations

Samples and irradiations

We irradiated pin-diodes of Cz-Si, standard Fz-Si and diffusion oxygenated Float Zone silicon. The summary of the diode materials used in this study is presented in Table 4.3. The diodes were first glued with photoresist to ceramic supports so that four diodes were placed on one support.

Table 4.3. Substrate materials used in this study.

Material	Manufacturer	Resistivity	Thickness	Diffusion oxygenation
Cz-Si	Okmetic	1100 Ωcm	380 μm	No
Fz-Si	Topsil	3 kΩcm	520 ± 20 μm	No
DOF	Topsil	3 kΩcm	520 ± 20 μm	Yes

Diodes were irradiated with 10 MeV and 20 MeV protons at Jyväskylä University Accelerator Laboratory, as described in Chapter 2.6. Six different proton doses were used: $5.9*10^{12}$, $1.2*10^{13}$, $1.8*10^{13}$, $3.0*10^{13}$, $5.9*10^{13}$, and $1.2*10^{14}$ protons/cm^2. For statistics, two similar samples were always exposed to each irradiation dose of both proton energies. Hardness factors 4.32 and 2.67, obtained from reference [28], were used when calculating the 1 MeV neutrons/cm^2 equivalent doses for the 10 MeV and 20 MeV irradiations, respectively. As a comparison, a dose of $1.6*10^{14}$ cm^{-2} 1 MeV neutrons/cm^2 is predicted for the inner parts of CMS silicon Tracker after 10 years of operation [29]. After the irradiations, the samples were kept refrigerated below room temperature.

Characterisation after irradiations

Full depletion voltages and the leakage currents were resolved by Capacitance-Voltage (CV) and Current-Voltage (IV) measurements, respectively. The results of the CV measurements are presented in Fig. 4.6. In order to simplify the comparison, the effective doping concentration was first calculated. Thus, the voltage values presented in Fig. 4.6 correspond to voltages required to deplete a 300 μm thick diode. The leakage currents of the irradiated diodes are presented in Fig. 4.7. The IV measurements were performed at a temperature of $(22^o \pm 0.5^o)$ C.

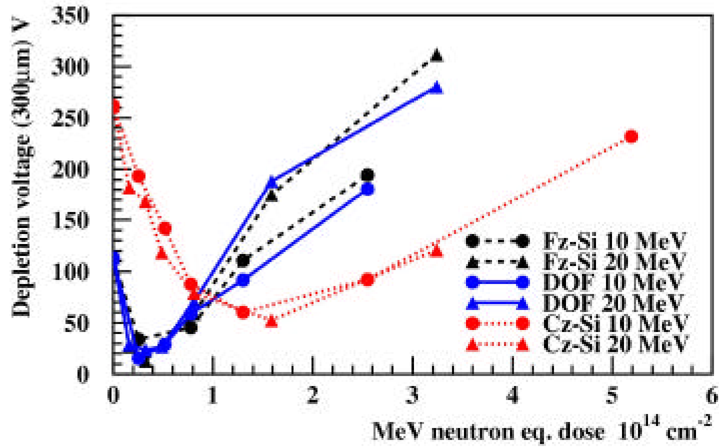

Figure 4.6. Full depletion voltages of Fz-Si, DOF and Cz-Si diodes irradiated with 10 and 20 MeV protons.

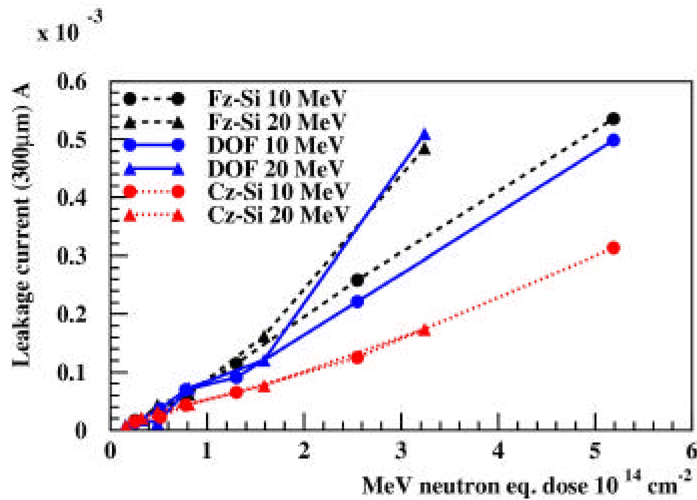

Figure 4.7. Full depletion leakage currents of Fz-Si, DOF and Cz-Si diodes irradiated with 10 and 20 MeV protons.

As seen in Fig. 4.6, the depletion voltage of Cz-Si is less sensitive to the increased radiation dose than the depletion voltage of standard Fz-Si or diffusion oxygenated Fz-Si, i.e. DOF. Even after the maximum dose of $5*10^{14}$ cm^{-2}, the depletion voltage of the Cz-Si diodes is less than the initial depletion voltage before irradiation. In Cz-Si silicon, the depletion voltage never falls to zero, which is a typical in low-resistivity silicon [27, p. 315]. As seen in Fig. 4.7, at corresponding irradiation doses, the leakage current of the Cz-Si diodes is lower than the leakage current of the Fz-Si diodes.

Additionally, according to the preliminary results, space charge sign inversion (SCSI) takes place in the Czochralski silicon material only after much higher irradiation doses than is the case with Float Zone silicon material. The SCSI naturally reduces the spatial resolution of the p-n segmented detectors. If Czochralski silicon material is used in large quantities, this unique feature has potential for a technological impact in the design of silicon detectors for the tracking systems of future High Energy Physics experiments [42].

Thus we can conclude that Cz-Si is more radiation hard than standard and oxygenated Fz-Si. The Cz-Si devices proved to be less sensitive to changes in the depletion voltage, as well as to the increase of leakage current, than the reference devices.

5 Conclusions

The purpose of this work was to develop radiation hard silicon detectors. Our approach was to improve the radiation hardness of the silicon material by increased oxygen concentration. We studied two different methods: diffusion oxygenation of Float Zone silicon as well as use of high resistivity Czochralski silicon.

Our research on diffusion oxygenated Float Zone silicon resulted in several interesting and previously unreported findings. We discovered an evident correlation between silicon oxygenation and detector leakage current. Additionally, we found that the oxygen concentration as well as the initial doping density of silicon material influences the recovery rate of meta-stable defect states.

We successfully applied alternative methods for the characterisation of silicon detectors, i.e. PCD (Photoconductivity Decay) and SPV (Surface Photovoltage). The PCD method was used to measure minority carrier lifetimes from oxidised wafers before irradiations, and the SPV method proved to be an excellent method for characterising irradiated silicon samples.

The most important results of our research were obtained in our work on high resistivity Czochralski silicon. Although the advantages of Cz-Si were known before, we were the first group to process, characterise, test in a particle beam, and irradiate full-size Czochralski silicon detectors.

In Czochralski silicon wafers, the beneficial effect of oxygen could clearly be seen by minority carrier lifetime characterisation using the PCD method. Obviously, the metallic impurities, i.e. process-induced contamination, are relatively effectively gettered into the oxygen precipitations present in the Czochralski silicon material.

Czochralski silicon detectors were found to be appropriate for particle detection, i.e. leakage currents were relatively low at full depletion, depletion voltages were reasonable, and no breakdown occurred near the depletion voltages. In particle beam tests, the particle detection performance of the Czochralski silicon detector, i.e. resolution, efficiency and signal-to-noise ratio, was shown to be comparable with the existing silicon strip detectors.

In proton irradiations, Czochralski silicon was found to be more radiation hard than standard or diffusion oxygenated Float Zone Silicon. Czochralski silicon devices proved to be less sensitive to changes in depletion voltage as well as to increase of leakage current. Additionally, according to the preliminary results, space charge sign inversion (SCSI) takes place in the Czochralski silicon material only after very high irradiation doses.

These findings related to radiation tolerance cannot be explained simply by the differences between the oxygen concentration in Czochralski silicon and oxygenated Float Zone Silicon. For example, oxygen-induced defect levels apparently interact with charged defects induced by proton irradiation. Comprehensive defect analysis is not within the scope of this work. However, efforts to explain these differences between Czochralski silicon and Float Zone Silicon are being conducted at CERN RD39 and RD50 collaborations.

References

[1] G. Lindstroem, M. Moll, and E. Fretwurst, *Radiation hardness of silicon detectors - a challenge from high-energy physics*, Nucl. Instr. & Meth. vol. **A426** (1999) 1-15.
[2] The Tracker Project, Technical Design Report, CERN/LHCC 98-6, CMS TDR 5.
[3] G. N. Taylor & al, *Radiation induced bulk damage in silicon detectors RD2 Collaboration*, Nucl. Instr. & Meth. vol. **A383** (1996) 144-154.
[4] Z. Li & al., *Investigation of the oxygen-vacancy (A-centre) defect complex profile in neutron irradiated high resistivity silicon junction particle detectors*, IEEE Trans. Nucl. Sci. **39** (6) (1992) 1730 - 1738.
[5] M. Moll, E. Fretwurst, and G. Lindstroem, *Leakage current of hadron irradiated silicon detectors - material dependence*", Nucl. Instr. & Meth. **A426** (1999) 87-93.
[6] CERN RD39 Research Programme, http://rd39.web.cern.ch/RD39/.
[7] CERN RD50 Research Programme, http://rd50.web.cern.ch/rd50/.
[8] W. Kern, Handbook of Semiconductor Wafer Cleaning Technology, Noyes Publications, NJ, 1993.
[9] Olli Anttila, Okmtic Oyj., Personal communication.
[10] ICECREM 4.2, User's Guide, Fraunhofer Institut fur Integrierte Schaltungen, Erlangen (1991)
[11] B. H. Lee at al., Appl. Phys. Lett. **76** (18) (2000) 2538-2540.
[12] D. Passeri et al., IEEE Trans. Nucl. Sci. **NS-47** (4) (2000) 1468.
[13] D. K. Schroder, Semiconductor Material and Device Characterisation, Wiley-Interscience Publication, 2nd edition (1998).
[14] S.M. Sze, Physics of Semiconductor Devices, John Wiley & Sons, 2nd edition (1981).
[15] D. K. Schroder, *Carrier Lifetimes in Silicon*, IEEE Trans. Electron Devices **44** (1997) 160-170.
[16] G. Zoth, *Aspects of Silicon Contamination Control by Lifetime*, in: D.C. Gupta et al. (Eds.), Recombination Lifetime measurements in Silicon, Vol. ASTM STP 1340, West Conshohocken, PA, USA (1998) 30-44.
[17] H. Hashizume et al. *Carrier Lifetime Measurements by Microwave Photoconductivity Decay Method,* in: D.C. Gupta et al. (Eds.), Recombination Lifetime measurements in Silicon, Vol. ASTM STP 1340, West Conshohocken, PA, USA (1998) 47-58.
[18] J. K. Schroder, *Recombination Lifetimes in Silicon,* in: D.C. Gupta et al. (Eds.), Recombination Lifetime measurements in Silicon, Vol. ASTM STP 1340, West Conshohocken, PA, USA (1998) 12-13.
[19] E. O. Johnson, *Measurement of Minority Carrier Lifetime with the Surface Photovoltage*, J. Appl. Phys. **28** (1957) 1349-1353.
[20] J. W. Orton and P. Blood, *The Electrical Characterisation of Semiconductors: Measurement of Minority Carrier Properties*, Academic Press Ltd. (1990) 72-77.
[21] I. Pintilie et al, *Thermally stimulated current method applied on diodes with high concentration of deep trapping levels*, Appl. Phys. Ltr. **78** (4) (2001) 550-552.
[22] C. Eklund et al. *Silicon Beam Telescope for CMS detector tests*. Nucl. Instr. and Meth. **A430** (1999) 321-332.
[23] K. Banzuzi et al. *Performance and calibration studies of silicon strip detectors in a test beam.* Nucl. Instr. and Meth. **A453** (2000) 536-544.
[24] Troll Tech, *Qt GUI software toolkit*, 1999.
[25] J. Kyriakopoulos and D. Reid, *Histo-Scope v4.0 User's Guide*, Fermilab SP0034 (1997).

[26] A. Virtanen, J. Hyvönen, K. Ranttila, I. Rekikoski and J. Tuppurainen, *Heavy ion and proton test site at JYFL-accelerator laboratory*, Nucl. Instr. and Meth. **A426** (1999) 68-71.
[27] G. Lindström & al., *Radiation hard silicon detectors - developments by the RD48 (ROSE) collaboration*, Nucl. Instr. and Meth. **A466** (2) (2001) 308-326.
[28] A. Vasilescu and G. Lindstroem, *Displacement damage in silicon, on-line compilation*, http://sesam.desy.de/~gunnar/Si-dfuncs.html.
[29] CMS Technical proposal, CERN/LHCC 94-38 (1994).
[30] P. A. Basore and D. A. Clugston, Proc. 25th IEEE Photovoltaic Specialists Conference (1996).
[31] D. Bechevet et al., *Results of irradiation tests on standard planar silicon detectors with 7-10 MeV protons*, Nucl. Instr. And Meth. **A479** (2002) 487-497.
[32] T. Abe and W. Qu, *High resistivity CZ silicon for RF applications substituting GaAs*, Electrochemical Society Proc. Vol. 2000-17 (2000) 491-500.
[33] B. Shen et al., Appl. Phys. Lettr. **70** (14) (1997) 1876-1878.
[34] B. Shen et al., J. Appl. Phys, **76** (8) (1994) 4540-4546.
[35] W. M. Bullis. Material Scien. and Eng. **B72** (2000) 93-98.
[36] V. Savolainen et al., Journal of Crystal Growth, Article in Press.
[37] W. O. Mara et al. (Eds.), Handbook of Semiconductor Silicon Technology, Noyes Publications (1990).
[38] D. V. Lang, *Deep-Level Transient Spectroscopy: a new method to characterise traps in semiconductors*, J. Appl. Phys. 45 (1974) 3023-3032.
[39] E. M. Verbitskaya, V. K. Eremin, A. M. Ivanov, N.B. Strokan, *Deep levels of thermal defects in high-resistivity ultrapure n-type silicon*, Sov. Phys. Semicond. **26** (1992) 1101-1106.
[40] C. T. Sah and C. T. Wang, J. Appl. Phys. **46** (1975) 1767.
[41] S. Braibant et al., *Investigation of design parameters for radiation hard silicon microstrip detectors,* Nucl. Instr. and Meth. **A485** (2002) 343-361.
[42] R. H. Richter & al, *Strip detector design for ATLAS and HERA-B using two-dimensional device simulation*, Nucl. Instr. and Meth. A377 (1996) 412-421.